AGU PUBLICATIONS

JGR

Journal of Geophysical Research: Oceans

RESEARCH ARTICLE

10.1002/2015JC011290

Special Section:
Forum for Arctic Modeling and Observing Synthesis (FAMOS): Results and Synthesis of Coordinated Experiments

Greenland freshwater pathways in the sub-Arctic Seas from model experiments with passive tracers

Dmitry S. Dukhovskoy[1], Paul G. Myers[2], Gennady Platov[3,4], Mary-Louise Timmermans[5], Beth Curry[6], Andrey Proshutinsky[7], Jonathan L. Bamber[8], Eric Chassignet[1], Xianmin Hu[2], Craig M. Lee[6], and Raquel Somavilla[9]

[1]Center for Ocean-Atmospheric Prediction Studies, Florida State University, Tallahassee, Florida, USA, [2]Department of Earth and Atmospheric Sciences, University of Alberta, University of Alberta, Edmonton, AB T6G 2E3, Canada, [3]Institute of Computational Mathematics and Mathematical Geophysics, Novosibirsk, Russia, [4]Department of Mathematical Geophysics, Novosibirsk State University, Novosibirsk, Russia, [5]Department of Geology and Geophysics, Yale University, New Haven, Connecticut, USA, [6]Applied Physics Laboratory, University of Washington, Seattle, Washington, USA, [7]Department of Physical Oceanography, Woods Hole Oceanographic Institution, Mail Stop 29/218B Clark Laboratory, Woods Hole, Massachusetts, USA, [8]Bristol Glaciology Centre, School of Geographical Sciences, University of Bristol, University Road, Bristol, UK, [9]Centro Oceanográfico de Gijón, Instituto Español de Oceanografia, Madrid, Spain

Abstract Accelerating since the early 1990s, the Greenland Ice Sheet mass loss exerts a significant impact on thermohaline processes in the sub-Arctic seas. Surplus freshwater discharge from Greenland since the 1990s, comparable in volume to the amount of freshwater present during the Great Salinity Anomaly events, could spread and accumulate in the sub-Arctic seas, influencing convective processes there. However, hydrographic observations in the Labrador Sea and the Nordic Seas, where the Greenland freshening signal might be expected to propagate, do not show a persistent freshening in the upper ocean during last two decades. This raises the question of where the surplus Greenland freshwater has propagated. In order to investigate the fate, pathways, and propagation rate of Greenland meltwater in the sub-Arctic seas, several numerical experiments using a passive tracer to track the spreading of Greenland freshwater have been conducted as a part of the Forum for Arctic Ocean Modeling and Observational Synthesis effort. The models show that Greenland freshwater propagates and accumulates in the sub-Arctic seas, although the models disagree on the amount of tracer propagation into the convective regions. Results highlight the differences in simulated physical mechanisms at play in different models and underscore the continued importance of intercomparison studies. It is estimated that surplus Greenland freshwater flux should have caused a salinity decrease by 0.06–0.08 in the sub-Arctic seas in contradiction with the recently observed salinification (by 0.15–0.2) in the region. It is surmised that the increasing salinity of Atlantic Water has obscured the freshening signal.

Key Points:
- Results from passive tracer model experiments are presented
- Greenland freshwater pathways and accumulation in the sub-Arctic seas are analyzed
- Meltwater influence on salinity change in the sub-Arctic is discussed

Supporting Information:
- Supporting Information S1

Correspondence to:
D. S. Dukhovskoy,
ddukhovskoy@fsu.edu

Citation:
Dukhovskoy, D. S., et al. (2016), Greenland freshwater pathways in the sub-Arctic Seas from model experiments with passive tracers, *J. Geophys. Res. Oceans*, *121*, doi:10.1002/2015JC011290.

Received 2 SEP 2015
Accepted 19 DEC 2015
Accepted article online 26 DEC 2015

1. Introduction

Observational and modeling studies indicate that the Greenland Ice Sheet and other Arctic land ice are melting at a rate that has dramatically increased since the early 1990s [*Pritchard et al*., 2009; *Velicogna*, 2009; *Gardner et al*., 2011; *Bamber et al*., 2012; *Box and Colgan*, 2013]. The volume of surplus freshwater discharge from Greenland into the sub-Arctic seas (Greenland, Iceland, Norwegian, Labrador seas, Baffin Bay, and the Subpolar region in the North Atlantic, Figure 1) since 1990 ($\sim$3200 km^3 by 2010) [*Bamber et al*., 2012] is steadily approaching the magnitude of the freshwater anomaly (10,000 km^3) advected into the North Atlantic during the 1970 Great Salinity Anomaly event (GSA) [*Dickson et al*., 1988], suggesting that this freshwater source may have a significant impact on ocean conditions in the region.

The sensitivity of the thermohaline circulation in the North Atlantic to freshwater balance has been widely discussed in the literature [*Stommel*, 1961; *Rooth*, 1982; *Manabe and Stouffer*, 1988; *Rahmstorf*, 1995; *Malmberg and Jonsson*, 1997; *Jahn and Holland*, 2013]. Considerable progress has been made in understanding the role of the thermohaline circulation in abrupt climate change from the paleoclimate perspective [e.g., *Manabe and Stouffer*, 1993, 1995; *Clark et al*, 2002], thus providing a link between the freshwater budget of the sub-Arctic and climate variability [*Stouffer et al*., 2006; *Dickson et al*., 2007; *Rahmstorf et al*., 2015].

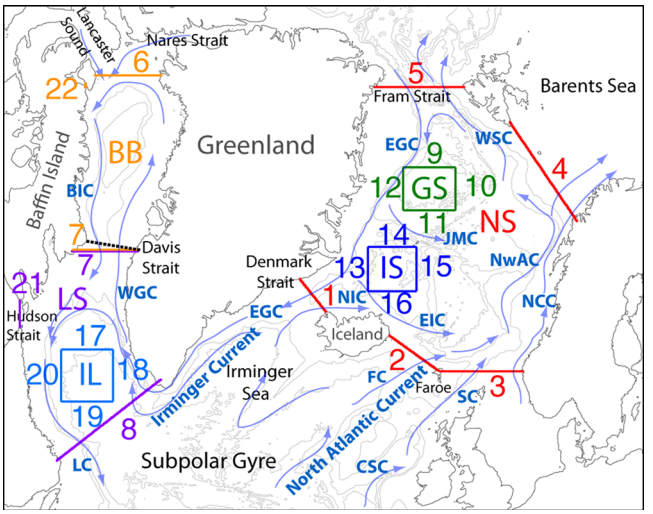

Figure 1. Map of the sub-Arctic seas with general circulation and geographic names shown, including the regions selected for tracer budget analysis (section 4). Three main basins include the Nordic Seas (NS), the Labrador Sea (LS), and Baffin Bay (BB). The boxes are interior regions in the Greenland Sea (GS), Iceland Sea (IS), and interior Labrador Sea (IL). The numbers indicate segments bounding the regions. Color coding is used for ease of identification of the segments bounding the regions. The dashed black line across Davis Strait shows the location of the 2004–present moored array. Abbreviated currents: CSC – Continental Slope Current, FC – Faroe Current, SC – Shetland Current, NCC – Norwegian Coastal Current, NwAC – Norwegian Atlantic Current, WSC – West Spitsbergen Current, EGC – East Greenland Current, JMC – Jan Mayen Current, EIC – East Icelandic Current, NIC – North Icelandic Current, WGC – West Greenland Current, BIC – Baffin Island Current, LC – Labrador Current.

The Arctic Ocean and the Greenland Ice Sheet are two sources of freshwater that potentially may impact the thermohaline circulation in the North Atlantic and influence the Atlantic Meridional Overturning Circulation (AMOC). Past GSA events resulting from anomalously high freshwater flux from the Arctic Ocean have been shown to have impacted thermohaline conditions and climate in the North Atlantic in the 20th century [*Dickson et al*., 1988; *Belkin*, 2004; *Curry and Mauritzen,* 2005]. Further, conceptual and idealized models have put forward mechanisms by which a freshwater flux from the Arctic Ocean may be a key factor in controlling the thermohaline circulation in the North Atlantic [e.g., *Ikeda*, 1990; *Mysak and Venegas*, 1998; *Ikeda et al*., 2001; *Goosse et al*., 2002; *Proshutinsky et al*., 2002; *Dukhovskoy et al*., 2004].

Meltwater from the Greenland Ice Sheet is the other major source of freshwater considered to influence thermohaline circulation and climate [*Rahmstorf*, 2002; *Fichefet et al*., 2003; *Rahmstorf*, 2003; *Ridley et al*., 2005; *Rudels*, 2011; *Castro de la Guardia et al*., 2015]. With growing evidence of accelerated Greenland ice melt [*Velicogna*, 2009; *Bamber et al*., 2012; *Box and Colgan*, 2013], increasing attention has been given to the role of meltwater in the high-latitude climate [*Hu et al*., 2011*; Weijer et al*., 2012; *Rahmstorf et al*., 2015]. *Proshutinsky et al*. [2015] conjecture that the recent observed disruption of quasidecadal oscillations of the Arctic wind-driven circulation regimes may be attributed to a surplus freshwater flux from Greenland. The underlying assumption is that a substantial volume of Greenland freshwater spreads laterally from the Greenland coast into convective sites of the interior sub-Arctic seas (regions GS, IS, and IL in Figure1). On the other hand, observational studies suggest that freshwater predominantly flows in boundary currents along the margins of the Nordic Seas (the East Greenland Current) and the Labrador Sea (the West Greenland Current and the Labrador Current) [e.g., *Bacon et al*., 2002; *Dickson et al*., 2007; *Sutherland and Pickart*, 2008; *Myers et al*., 2009]. Hence, most of the Greenland freshwater discharge should travel along the margins of the sub-Arctic seas on its way to the North Atlantic (Figure 1). It remains unclear how, where, and on what timescales this freshwater can impact convective regions [*Moore et al*., 2015]. The rate of Greenland freshwater flux into the interior seas, which is unknown, is also important. Previous model experiments have shown that the thermohaline circulation in the North Atlantic responds to freshwater perturbations on order of 0.1 Sv [*Rahmstorf*, 1995; *Fanning and Weaver*, 1997; *Clark et al*., 2002].

In order to understand the mechanisms of climate change driven by changes in AMOC in response to increased ice sheet melting, a number of "hosing" experiments have been performed with Ocean General Circulation Models and climate models [*Huybrechts et al*., 2002; *Fichefet et al*., 2003; *Ridley et al*., 2005; *Jungclaus et al*., 2006; *Gerdes et al*., 2006; *Stouffer et al*., 2006; *Swingedouw et al*., 2006; *Vizcaino et al*., 2008; *Hu et al*., 2011]. Overall, these experiments show different AMOC states as a function of freshwater flux into the North Atlantic. These numerical experiments are not designed to address any of the questions raised above. Typically in these hosing experiments surplus freshwater flux is imposed over some region of the North Atlantic. Although such simplification of freshwater input into the North Atlantic seems to have low impact on climate simulations [*Kleinen et al*., 2009], misrepresentation of actual pathways of Greenland freshwater

into the ocean may be important for the realistic responses of thermohaline processes in the sub-Arctic seas, as discussed in *Stammer* [2008], *Marsh et al*. [2010], and *Weijer et al*. [2012].

In order to investigate the influence of surplus Greenland Ice Sheet meltwater on the sub-Arctic seas and North Atlantic, several high-resolution ocean experiments have been conducted. A model study of *Marsh et al*. [2010] includes 0.25° and 1° NEMO simulations integrated for 8 years. They found that the freshwater signal tends to stay along the narrow boundary current of the Labrador Sea and only a small volume of freshwater has reached the interior Subpolar Gyre in the simulation after 8 years. The largest volume of surplus freshwater accumulated in Baffin Bay. The authors mention that the East Greenland Coastal Current, which acts as a freshwater conduit, is not resolved in the NEMO experiments. *Bacon et al*. [2014] conclude that at least 1/12° model resolution is needed to resolve freshwater fluxes associated with East Greenland Coastal Current.

Another recent model study of *Weijer et al*. [2012] compares the adjustment of the AMOC to the surplus of Greenland freshwater in multidecadal simulations with 0.1° ("strongly eddying") and 1° ("non-eddying") global configurations from the Los Alamos Parallel Ocean Program (POP). In these experiments, a passive tracer is released along with the freshwater anomaly around Greenland in order to diagnose the freshwater propagation rate. The numerical experiments predict rapid spreading of the tracer at shallow depths over the sub-Arctic seas (within a year) with a distinct delay (about a year) in the arrival time for the tracer in the interior Nordic Seas. The strongest freshening is simulated in the Labrador Sea and Baffin Bay, whereas the decline in surface salinity in the Nordic Seas is much weaker.

The goal of this paper is to investigate the pathways, mechanisms, and time scales of Greenland meltwater propagation within the sub-Arctic seas with particular focus on the Nordic Seas, the Labrador Sea, and Baffin Bay (Figure 1). We start our analysis with a description of the Greenland Ice Sheet runoff data used in the model experiments (section 2) and a brief overview of observed salinity changes in the sub-Arctic seas that could provide evidence of the influence of surplus Greenland freshwater influence (section 3). Design and analysis of numerical experiments employing three regional coupled ocean-sea ice models with different resolution forced by realistic Greenland freshwater fluxes are discussed in section 4. The experiments use a passive tracer released at exact locations of the Greenland freshwater sources. The model results are analyzed from the perspective of observed salinity changes in the sub-Arctic seas (section 5).

2. Greenland Freshwater Flux

2.1. Data

Greenland freshwater fluxes, between 1958 and 2010, from *Bamber et al*. [2012] are employed to investigate the fate of this freshwater and assess its role in thermohaline variability over the past decade. The data are a monthly gridded product (5 × 5km grid) with realistic geographic distribution and temporal variability (Figure 2a). Greenland runoff was derived from a reconstruction of the surface mass balance of the Greenland Ice Sheet and surrounding tundra using a high-resolution regional climate model, RACMO2 [*Ettema et al*., 2009] forced with ERA-40 re-analysis data. The runoff from the ice sheet and surrounding tundra was combined with observations of solid ice discharge derived from satellite observations of ice velocity to produce the total freshwater flux to the ocean.

2.2. Variability and Trends, 1990–2010

According to *Bamber et al*. [2012], total Greenland freshwater flux has been predominantly >1000 km^3 yr^{-1} since 1998 having increased from 870 to 900 km^3 yr^{-1} in the early 1990s to 1100 to 1200 km^3 yr^{-1} in the late 2000s (Figure 2b). A somewhat smaller estimate of the total Greenland freshwater flux is reported in *Box and Colgan* [2013], but it did not include tundra runoff that accounts for an additional 100–200 km^3 yr^{-1}. However, their estimate indicates a similar increase of the Greenland freshwater flux of around 200 km^3 yr^{-1} between 1990 and 2010.

The volume of freshwater supplied by the Greenland Ice Sheet is roughly 29%–42% of the total annual river runoff into the Arctic Ocean (3500 km^3 yr^{-1} according to *Curry and Mauritzen* [2005] or 2500 km^3 yr^{-1} as reported by *Aagaard and Carmack* [1989] based on climatological data of the 1980s) [*Serreze et al*., 2006; *Bamber et al*., 2012]. The change of the freshwater flux between 1990 and 2010 is equivalent to a freshwater input increase of 6.3–10.5 mSv. This increase is smaller than those of an earlier study of *Gregory and Lowe*

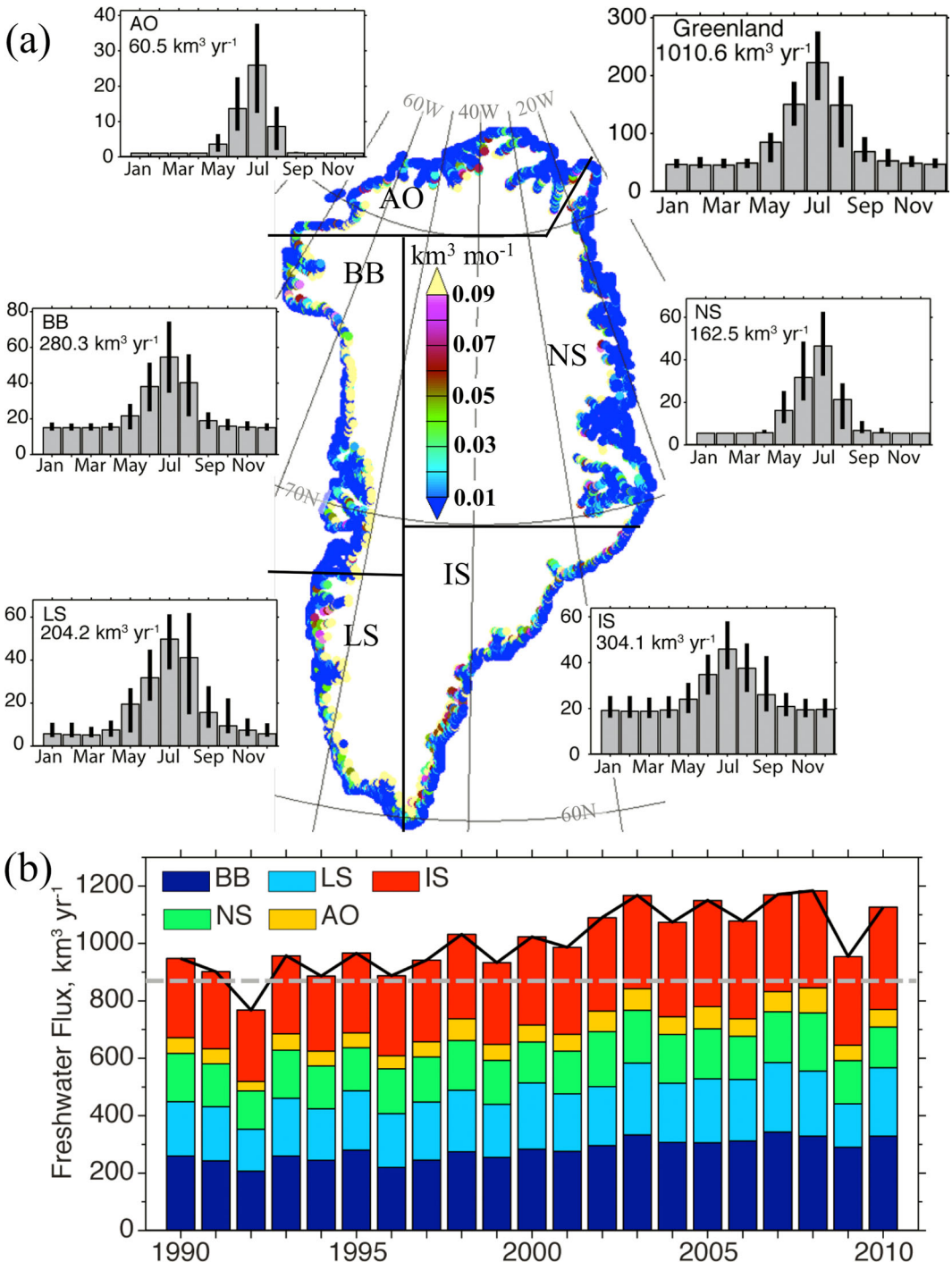

Figure 2. Seasonal and interannual variability of Greenland freshwater fluxes from *Bamber et al.* [2012], 1990–2010. The fluxes include both solid and liquid discharge. (a) Locations and volume fluxes ($km^3\ mo^{-1}$) of Greenland freshwater sources along the coast. The bar diagrams show monthly averaged Greenland freshwater fluxes between 1990 and 2010 ($km^3\ mo^{-1}$) integrated over the regions delineated with the black lines. At the upper right, monthly runoff integrated over the whole Greenland coast is shown. The vertical black lines on top of the bars indicate the range of the monthly runoff during 1990–2010. Long-term (1990–2010) mean runoff ($km^3\ yr^{-1}$) is listed for every region. (b) Stacked bar diagram of the annual Greenland freshwater flux in the regions. The black line depicts the total annual freshwater flux. The grey-dashed line shows the total Greenland discharge averaged over 1961 through 1990 (876 $km^3\ mo^{-1}$).

[2000] noting a 17.4 mSv increase. In addition, between 2004 and 2009 mass loss from the Canadian Arctic Archipelago (CAA), primarily into Baffin Bay, changed from 31 to 92 $km^3\ yr^{-1}$ [*Gardner et al*, 2011], an increase from about 1–3 mSv.

Estimated from the Greenland freshwater data of *Bamber et al*. [2012], the cumulative Greenland freshwater flux anomaly between 1990 and 2010 is 2830 ± 337 km^3 relative to the pre-1990 mean flux of 876 km^3 yr^{-1}. This amount is 28% of the freshwater volume advected to the sub-Arctic from the Arctic Ocean during the 1970s GSA event, totaling 10,000 km^3 [*Dickson et al*., 1988]. If the Greenland freshwater flux increases at the same rate for the next 50 years, the surplus freshwater will reach the GSA freshwater volume by the mid-2060s. It is noteworthy that rates of mass loss from Greenland have been steadily increasing since 2010 [*Helm et al*., 2014].

3. Observed Salinity Changes in the Sub-Arctic Seas

Recent changes in salinity fields in the sub-Arctic seas are discussed below in an attempt to identify observational evidence of the presence of freshwater released from Greenland that has been increasing since the early 1990s.

3.1. Baffin Bay

Hydrographic characteristics of Baffin Bay are largely determined by outflow from the Arctic Ocean and inflow from the Labrador Sea that enters the bay as the West Greenland Current (WGC, Figure 1). Greenland freshwater flux to Baffin Bay has substantially increased since the early 1990s (200–250 km^3 yr^{-1}) contributing about 316 km^3 yr^{-1} in the late 2000s (Figure 2b). This is ~13% of the freshwater transport through the northern channels of the Canadian Arctic Archipelago (CAA) estimated as 2450 km^3 yr^{-1} combining estimates in *Peterson et al*. [2012], *Münchow and Melling* [2008], *Rabe et al*. [2012], *Agnew et al*. [2008], and *Kwok* [2007].

A detailed analysis of hydrographic changes in Baffin Bay over 1916–2003 based on historical data was conducted by *Zweng and Munchow* [2006]. The majority of the observations used were collected between 1950 and the early 2000s. The study revealed significant freshening over the shelf and slope regions of Baffin Bay in the layer between 50 and 200 m depth range. The largest freshening (-0.086 ± 0.039 decade^{-1}) was found on the Baffin Island shelf. A smaller freshening (from -0.048 to -0.066 decade^{-1}) was reported for the continental slopes off Baffin Island. The surface waters of the Greenland shelf and slope regions to the north of Davis Strait had similar freshening trends (-0.04 decade^{-1}). The authors suggest Greenland meltwater runoff might have contributed to this freshening. Recently *Myers and Ribergaard* [2013] also found freshening in the upper layer of Disko Bay, as well as offshore in the West Greenland Current in the 2000s as compared to the 1980s and 1990s.

Moored observations in Davis Strait described in *Curry et al*. [2014] indicate slight freshening of several water mass classes (Figures 3a–3c). Although no statistical significance can be drawn from these short time series, all but two water masses (West Greenland Irminger Water, WGIW and Transitional Water, TrW) tend to have negative salinity anomalies in recent years relative to the 2003–2013 mean (Figures 3b and 3c). UK Met Office Hadley Centre monthly salinity data (version EN.4.1.1) [*Good et al*., 2013] have been examined in the region (Figure 3d). Salinity anomalies relative to the 1960–1990 monthly climatology indicate apparent freshening signal in the upper 50 m over 1990–2014 in Baffin Bay. Over the past decade, fresh surface water has expanded southwards (by about 10° latitude) into the northern Labrador Sea.

3.2. The Labrador Sea

The Labrador Sea receives freshwater exported from the Arctic Ocean through the CAA via Davis Strait and Hudson Strait and through Fram Strait with the East Greenland Current (EGC) and the West Greenland Current (WGC) (Figure 1). Additionally, the Labrador Sea also receives saline modified Atlantic Water originating from the North Atlantic Current (called the Subpolar Mode Water in *McCartney and Talley* [1982]). The warm and saline Atlantic water flows along the continental slope around the basin as the Irminger Current. It is generally accepted that eddies shed by the Irminger Current control the heat and salt budget of the interior Labrador Sea [e.g., *Straneo*, 2006], governing winter convective activity when the intermediate and deep waters of the North Atlantic are formed [*Lazier et al*., 2002]. Deep convection controls formation and properties of Labrador Sea Water that occupies the central Labrador Sea [*Talley and McCartney*, 1982]. Deep winter convection in 1987–1994 produced an anomalously high volume of cold (<2.8°C) and fresh (<34.84) Labrador Sea Water [*Yashayaev*, 2007]. After 1994, the freshening of the water column reversed, especially in the

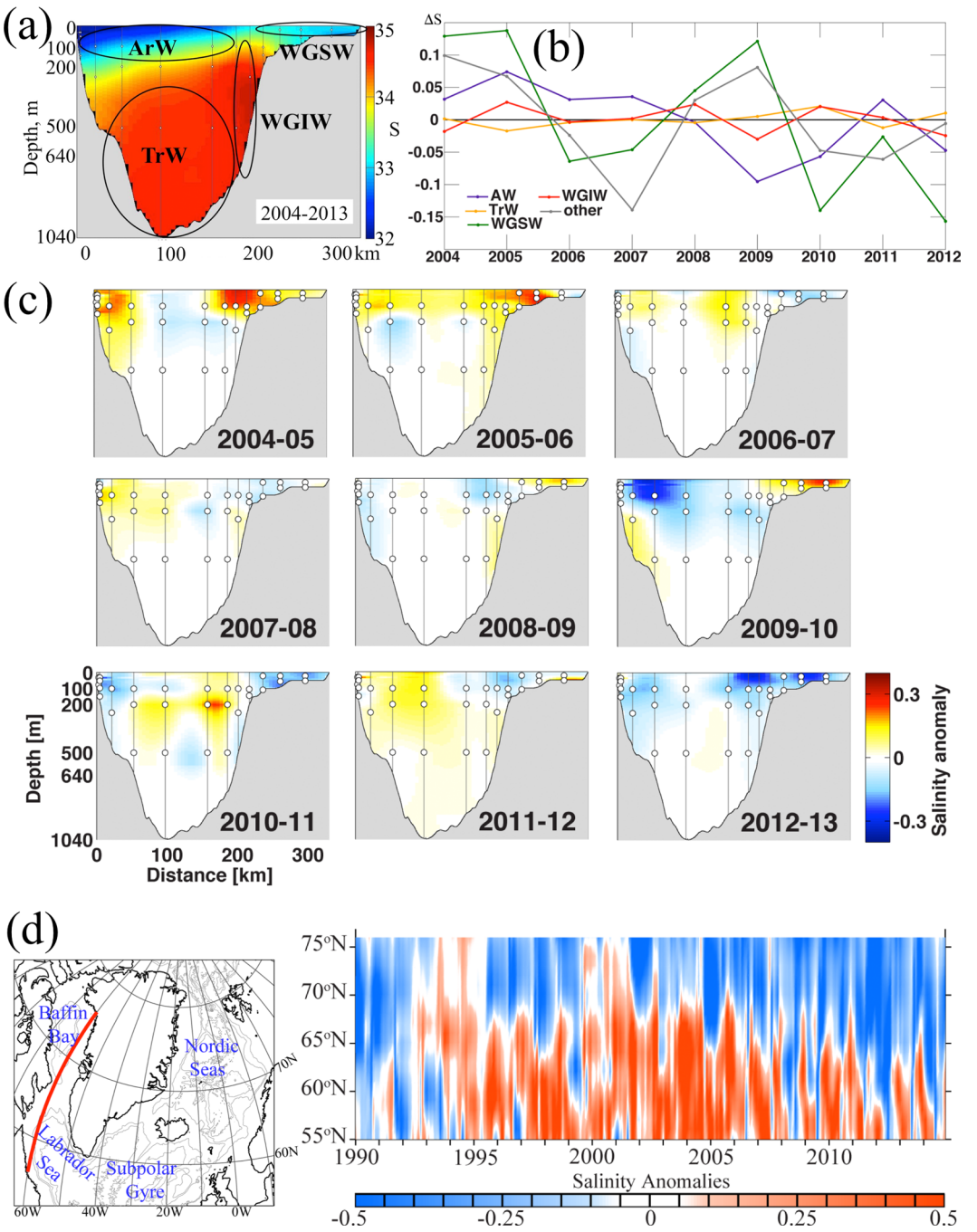

Figure 3. Mean salinity and salinity anomalies derived from the observational program in Davis Strait data between 2004 and 2013 (the location of the moored array is shown in Figure 1). (a) Mean salinity. The major water masses are indicated: ArW – Arctic Water, TrW – Transitional Water, WGIW – West Greenland Irminger Water, WGSW – West Greenland Shelf Water. (b) Annual salinity anomalies (ΔS) relative to the 2004–2013 mean for the individual water masses. The other water mass refers to the near surface water that is too warm to be classified as ArW or is near surface water along the West Greenland slope right at the shelf that is too salty to be WGSW and too fresh to be WGIW. (c) Annual salinity anomalies relative to the 2003–2013 mean. (d) Time versus latitude diagram showing salinity anomalies along the section shown with the red line on the map to the left for the time period from 1990 to 2014 relative to the 1960–1990 monthly climatology. Salinity climatology and anomalies are derived from the Met Office Hadley Centre subsurface ocean salinity data set (EN.4.1.1).

layers below 1000 m attributed to weaker convection in the central Labrador Sea with exception to the deep convection events during winter of 2007–2008 [*Yashayaev and Loder*, 2009].

Hydrographic observations in the central Labrador Sea indicate considerable variability of the temperature and salinity characteristics of the Labrador Sea Water over the last four decades [*Yashayaev*, 2007].

Oceanographic monitoring of the Labrador Sea was mostly done on the basis of annual hydrographic sections across the central Labrador Sea (for more details, see *Yashayaev* [2007]) until 2002 when the international Argo program (http://www.argo.ucsd.edu) was launched. In the early 1970s, the Labrador Sea had a noticeable freshening trend that continued until 1995 [*Dickson et al*., 2002; *Zweng and Munchow*, 2006; *Yashayaev and Seidov*, 2015]. During 1988 through 1994, strong freshening was observed in the upper 1500 m in the Labrador Sea caused by the formation of a large volume of cold and fresh Labrador Sea Water [*Sy et al*., 1997; *Lazier et al*., 2002]. After 1995, the salinity trend changed to positive and remained positive at least through the late 2000s. *Yashayaev and Loder* [2009] analyzed time evolution of hydrography fields in the central Labrador Sea on the basis of the Argo float data and in situ observations. Their results demonstrated a strong positive salinity anomaly developed in the 200–500 m layer during 2000–2009 with the highest salinity $>$34.9 in 2008 (compared to 34.78–34.82 in the late 1980s). Recent Argo observations in the Labrador Sea show a slight decrease in salinity in the 200–800 m layer after 2012 caused by several deep convection events, with the strongest convection occurred in 2014 [*Kieke and Yashayaev*, 2015]. Freshening in the upper 200 m has been observed in the western Subpolar Gyre region and the Labrador Sea since 2010 [*Beszczynska-Moller and Dye*, 2013; *Yashayaev et al*., 2015].

3.3. The Nordic Seas

Hydrographic characteristics of the upper ocean water masses in the Nordic Seas (NS in Figure 1) are influenced by the northward flowing Atlantic Water and southward flowing Polar Water from the Arctic Ocean carried by the EGC [*Aagaard et al*., 1985]. Whereas the eastern and western parts of the Nordic seas are largely determined by the characteristics of the Polar Water and Atlantic Water, respectively, the interior part, that includes convective regions in the Iceland and Greenland seas (IS and GS in Figure 1), has a more complex relationship between hydrography and contributions from Polar Water and Atlantic Water. The Greenland and Iceland seas have many features in common [*Malmberg and Jonsson*, 1997]. Hydrography of the upper layer in both seas is determined by water mass transformations and modifications through lateral advection of Polar Water and Atlantic Water from the rims of the seas and convection driven by surface cooling and salt flux during ice formation. The North Atlantic water undergoes substantial cooling and freshening as it mixes with the ambient water before entering the Greenland Gyre. Upon mixing, the two water masses form the upper Greenland and Iceland water mass, sometimes called Arctic Surface Water [*Carmack*, 2000].

Large salinity changes have been observed in the Nordic Seas since the 1950s. A long-term freshening of the North Atlantic in surface, intermediate, and deep water masses has been reported in *Dickson et al*. [2002], *Curry et al*. [2003], and *Curry and Mauritzen* [2005]. Hydrographic observations conducted in the Greenland and Iceland seas (regions "GS" and "IS" in Figure 1) reveal strong negative salinity anomalies ($<$34.3–34.5) in the upper 25 m layer during the late 1960s–1970s, late 1980s, and the late 1990s (Figure 4). The anomalies are related to the 1970s, 1980s, and 1990s GSAs, respectively [*Dickson et al*., 1988; *Belkin et al*., 1998; *Belkin*, 2004]. In the mid-2000s, high salinity ($>$34.7) was observed in both seas in the layer from 0 to 200 m. The positive salinity event was replaced by a strong freshening signal ($<$34.5) in 2008 in the upper Greenland Sea (above 50 m) but not in the Iceland Sea (Figure 4). A persistent salinity increase in the layers below 50–75 m was observed in the regions, especially apparent in the Greenland Sea. The observations in Figure 4 agree with the previous studies that reported a positive salinity trend in the Nordic Seas since the late 1990s [*Avsic et al*., 2006; *Hátún et al*., 2005; *Holliday et al*., 2008; *Somavilla et al*., 2013]. Recent analysis of Argo float observations in the Greenland and Iceland seas, between 2001 and 2007, shows a slightly positive salinity trend for the upper 500 m [*Latarius and Quadfasel*, 2010]. Increased salinity in the upper Nordic Seas is related to increased salinity in the Atlantic water flowing into the sub-Arctic seas [*Walczowski and Piechura*, 2006; *Holliday et al*., 2008; *Yashayaev and Seidov*, 2015], likely linked to increased salinity in subtropical and midlatitudes Atlantic Water [*Hátún et al*., 2005].

To summarize, historic observations in Baffin Bay show persistent freshening over the last two decades, whereas salinity in the other sub-Arctic seas has both positive and negative anomalies. Thus, no definite conclusion can be made on the linkage between observed salinity anomalies in the sub-Arctic seas and increased Greenland freshwater discharge observed during last decades. We believe that more information and additional studies are needed to reveal mechanisms and processes regulating freshwater fluxes and fresh water transformations under different complex processes. A better knowledge about freshwater pathways, accumulation rates, and time scales of freshwater propagation is necessary in order to understand

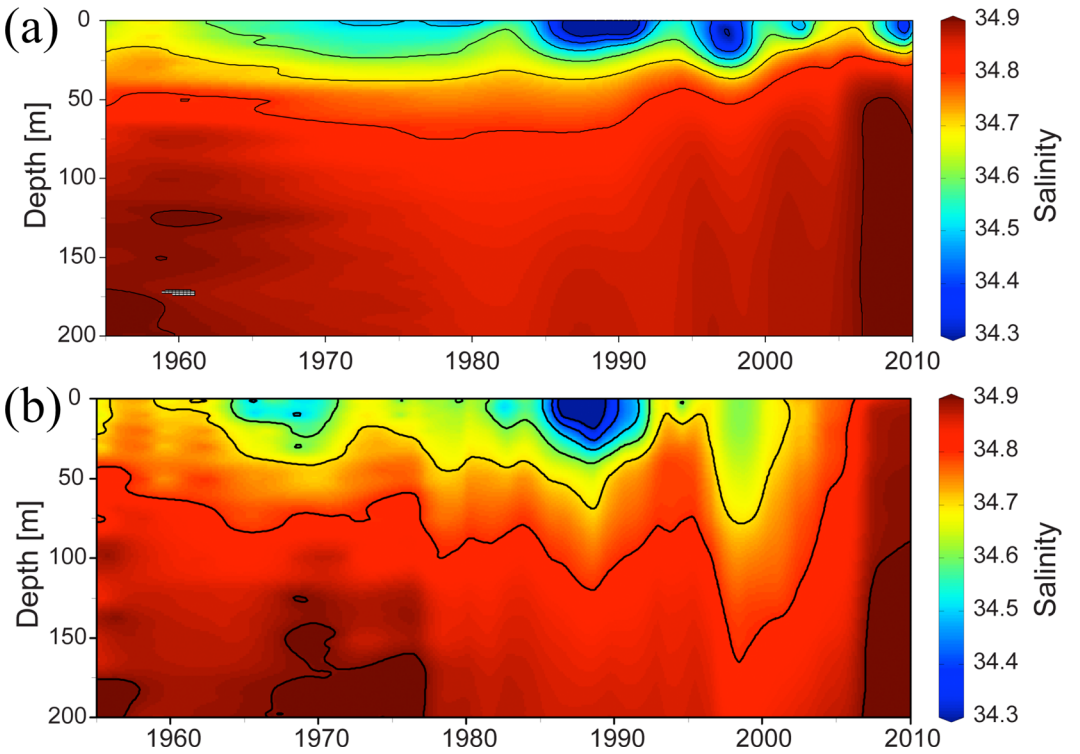

Figure 4. Time-depth diagrams of salinity in the central Greenland Sea (a) and Iceland Sea (b) from hydrographic observations in boxes GS and IS shown in Figure 1. Hydrographic measurements (salinity, temperature, and pressure from bottle and CTD data) in the Greenland and Iceland seas from 1950 to 2010 are from the ICES Data set on Ocean Hydrography (www.ocean.ices.dk) and the Pangaea database (www.pangaea.de). Note a very shallow (upper 25 m) freshening signal at both locations.

the disagreement between proposed freshening of the sub-Arctic seas caused by surplus Greenland freshwater flux and the observed salinity changes. Note that observational studies referenced in this section were primarily focused on hydrographic changes in the water column below the near-surface layer (upper 50–200 m). However, results from model experiments with passive tracers described in the following sections suggest that Greenland freshening should primarily manifest in the upper 200 m and mostly in the 0–50 m layer.

4. Results From the Passive Tracer Experiments

Three groups participating in the Forum for Arctic Ocean Modeling and Observational Synthesis (FAMOS) project have run ocean-sea ice models with passive tracers released at the Greenland freshwater sources. The models used in this study are from the Florida State University (AO-HYCOM), the University of Alberta (NEMO-LIM2), and the Institute of Computational Mathematics and Mathematical Geophysics (ICMMG). The simulations have different model forcing and configurations. The length of integration is 14 years. The models have different resolutions; AO-HYCOM has a high-resolution (0.08°) configuration and NEMO-LIM2 and ICMMG have 0.25° and 0.5° grid spacing, respectively. The only coordinated forcing is the Greenland freshwater flux data (described in section 2.1). In the model experiments, Greenland freshwater is tracked by a passive tracer released at the locations of Greenland freshwater sources (Figure 2a). The tracer is treated as a scalar variable and its time evolution is described by scalar advection and diffusion equations similar to temperature and salinity. Specifics of the models and experiments are summarized in Appendix A and Table A1.

4.1. Evolution of Tracer Concentration in the Upper Ocean

Time evolution of the passive tracer concentration in the simulations (Figures 5–7) reveals general agreement among the models. In particular, during the first several years, the models simulate rapid spreading of the freshwater tracer into the Labrador Sea (mainly with the Labrador Current) and Baffin Bay where the highest concentration is maintained throughout the simulation. On the eastern side of Greenland, the tracer is exported from the Nordic Seas by the EGC into the Labrador Sea and the Subpolar Gyre region, and then

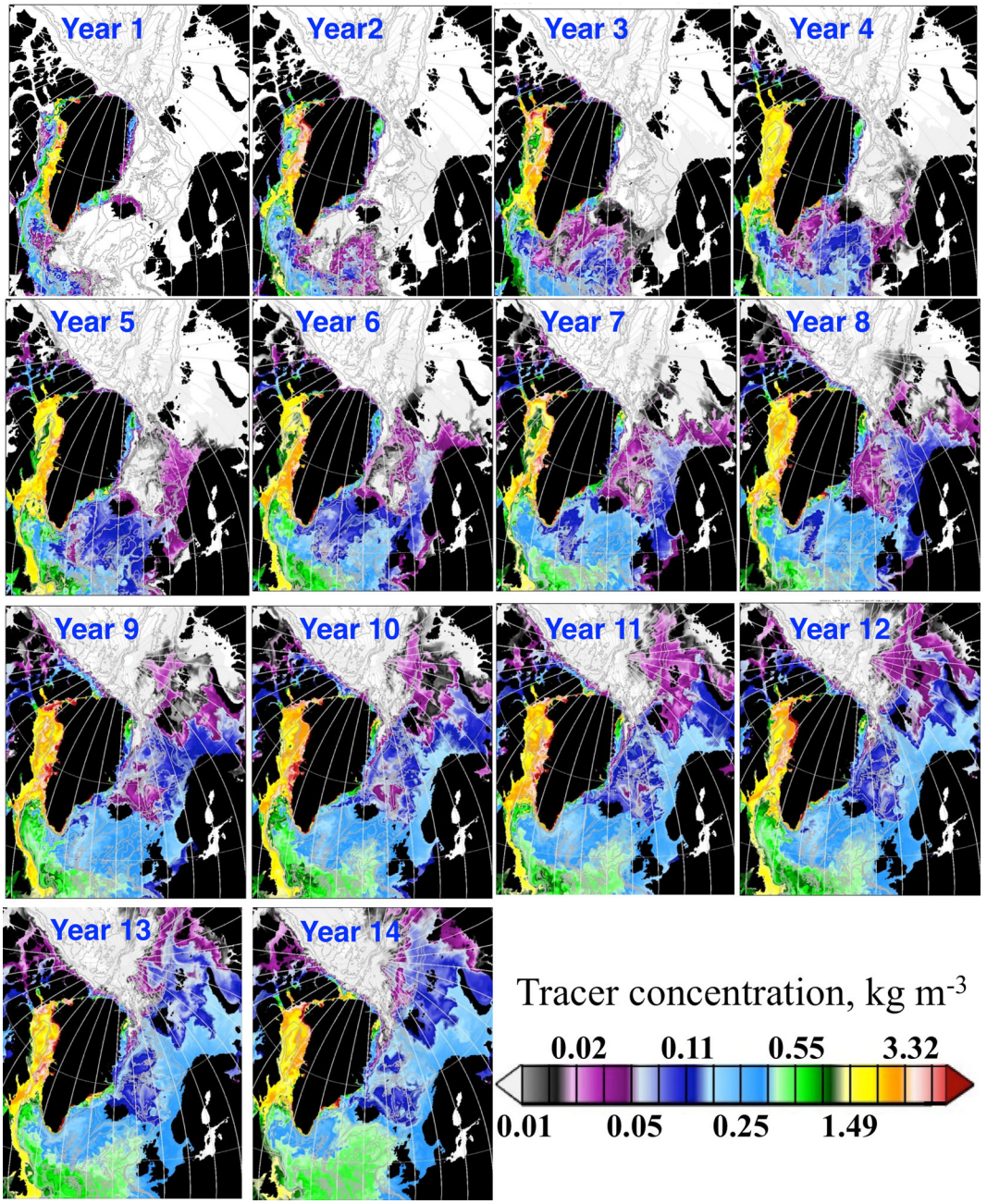

Figure 5. Daily mean tracer concentration in the first model layer (~3 m) on 17 December for every model year from AO-HYCOM. The concentration is on the natural-log scale (kg m^{-3}). See animated fields of daily mean tracer concentration from AO-HYCOM in Supporting information.

the tracer is advected back into the Nordic Seas with the North Atlantic current. Yet there are obvious discrepancies in the simulated fields. The differences among the models are found in tracer concentration in the sub-Arctic seas, tracer pathways, and spreading into the interior basins, and timing of tracer advection into the Nordic Seas.

Specifically, during the first 5 years of the AO-HYCOM simulation the tracer stays within the EGC. There is an indication of some advection of the tracer with the East Icelandic Current to the east (Years 1, 2, 5, and 6). However, the interior Nordic Seas show no signature of the tracer until year 6. After that, the interior Nordic Seas slowly fill up with the tracer being brought by the North Atlantic Current after the tracer has traveled around the Subpolar Gyre (Figure 5).

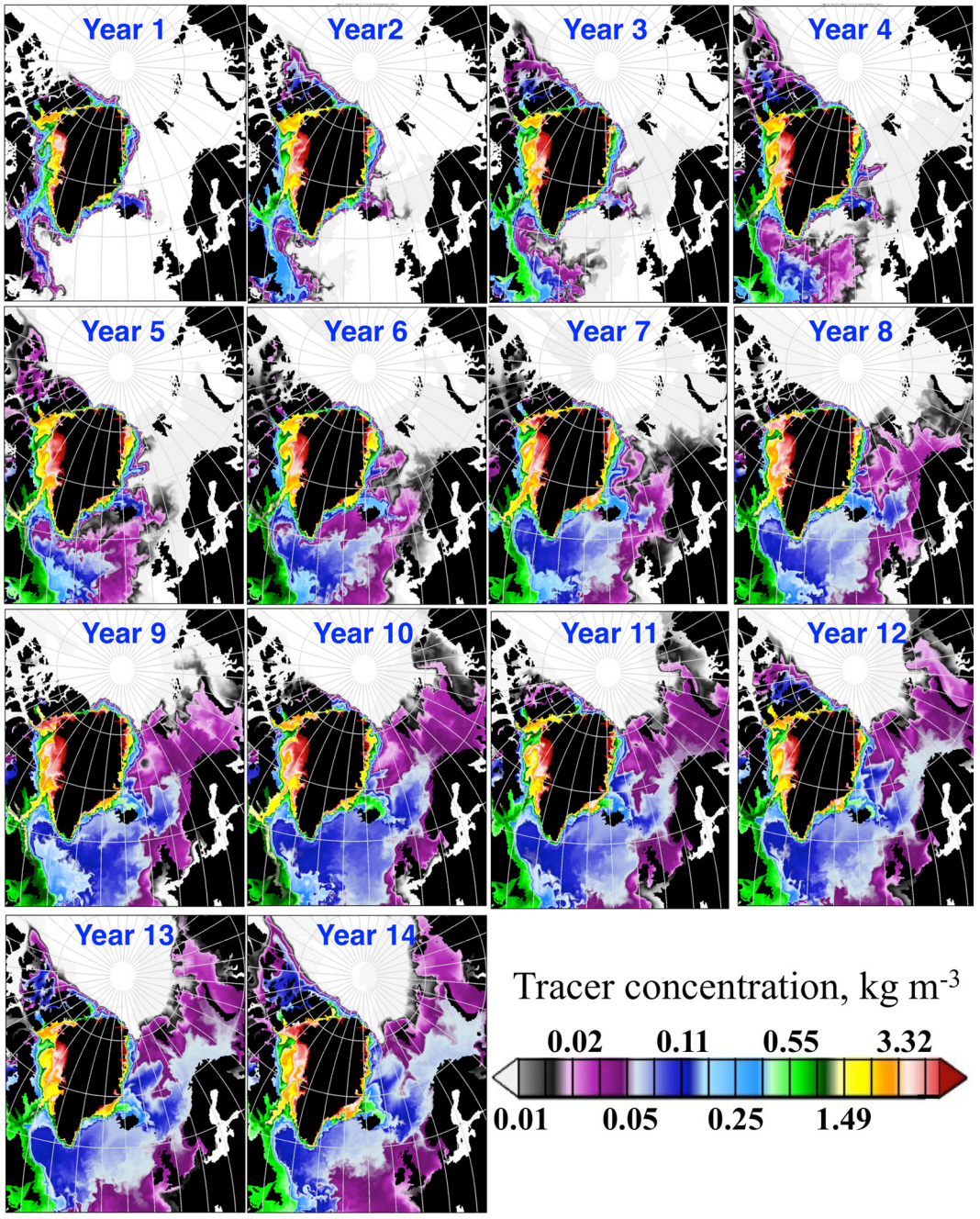

Figure 6. Five-day mean tracer concentration in the surface model layer (~1 m) for output including 17 December for every model year from NEMO-LIM2. The concentration is on the natural-log scale (kg m^{-3}).

The NEMO-LIM2 simulation (Figure 6) agrees with AO-HYCOM showing very limited lateral advection of the tracer off the EGC during the first 5 years of the simulation. Yet in contrast to AO-HYCOM, tracer spreading into the interior Nordic Seas by means of the west-to-east Jan Mayen current is evident in NEMO-LIM2. The timing of tracer propagation into the convective regions of the Nordic Seas is remarkably similar between the two models. Nevertheless, there is a notable distinction in how this propagation is simulated. In NEMO-LIM2, the tracer spreads from the south with the North Atlantic Current and from west off the EGC, whereas in AO-HYCOM the tracer is mainly advected by the North Atlantic Current.

The ICMMG simulation (Figure 7) qualitatively agrees well with both AO-HYCOM and NEMO-LIM2. Yet the ICMMG simulation does not predict any substantial tracer spreading off the EGC into the interior Nordic

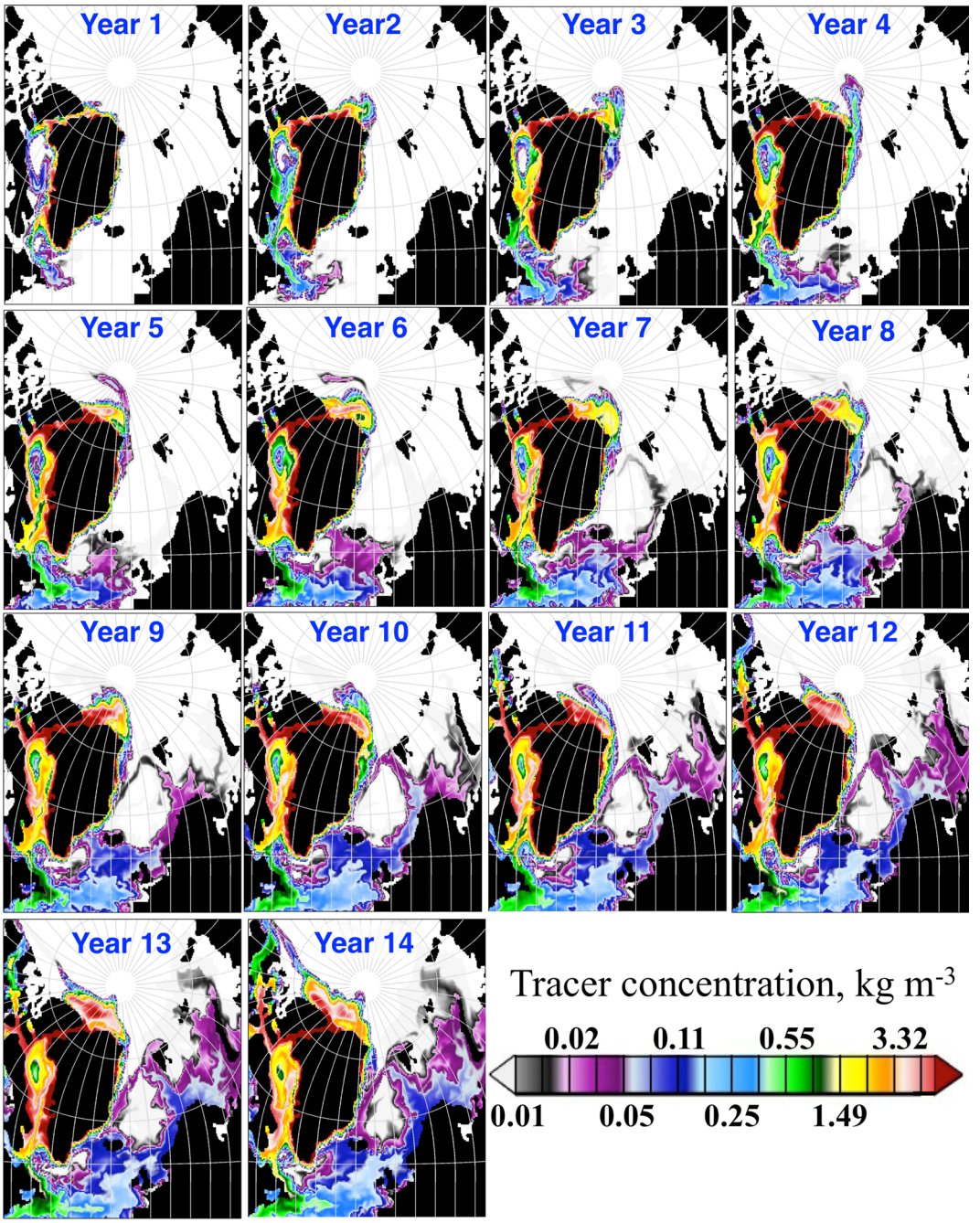

Figure 7. Daily mean tracer concentration in the surface model layer (~2 m) on 17 December for every model year from ICMMG. The concentration is on the natural-log scale (kg m^{-3}).

Seas, unlike the NEMO-LIM2 simulation. In ICMMG, it takes much longer (10 years) for the tracer to travel around the Subpolar Gyre before returning to the Nordic Seas with the North Atlantic Current, compared to AO-HYCOM and NEMO-LIM2. Another discrepancy between ICMMG and the two other models is sluggish propagation of the tracer into the interior of the basins in the ICMMG simulation. For example, propagation of the tracer in Baffin Bay is predominantly along the coast in the ICMMG simulation. By contrast, there is substantial lateral advection of the tracer into the interior Baffin Bay in both AO-HYCOM and NEMO-LIM2. Similarly in the Labrador Sea and the Nordic Seas, ICMMG simulates a slower rate of tracer spreading into the interior basins.

Another disagreement between ICMMG and the two other models is the evolution of the tracer concentration to the north and west off Greenland. ICMMG simulates an extensive spread of the tracer into the Arctic Ocean

from the northern Greenland coast, whereas in both AO-HYCOM and NEMO-LIM2 simulations tracer propagation into the Arctic Ocean is limited and confined to the narrow shelf north of Greenland and the CAA.

4.2. Tracer Budget Analysis

In order to characterize propagation and accumulation of the tracer in the sub-Arctic seas, a tracer budget is calculated for the six regions shown in Figure 1. The study area is divided into three basins: the Nordic Seas (NS), the Labrador Sea (LS), and Baffin Bay (BB). Within the NS and LS, convective sites in the Greenland Sea (GS), the Iceland Sea (IS), and interior Labrador Sea (IL) are designated. For each region, passive tracer storage (volume-integrated tracer content or mass, M_{tr}) is calculated as

$$M_{tr}(t) = \iiint_V C_{tr}(x, y, z, t)\ dV, \tag{1}$$

where C_{tr} is tracer concentration (kg m^{-3}). Within a region, tracer fluxes (F_{tr}) are estimated for each segment bounding the region by integrating over the total water depth (H) along the segment l of length L

$$F_{tr} = \int_L \int_H C_{tr}(l, z, t)\ \mathbf{u}(l, z, t) \cdot \mathbf{n}(l)\ dz\ dl, \tag{2}$$

where **n** is an inward unit normal vector (positive flux into the region).

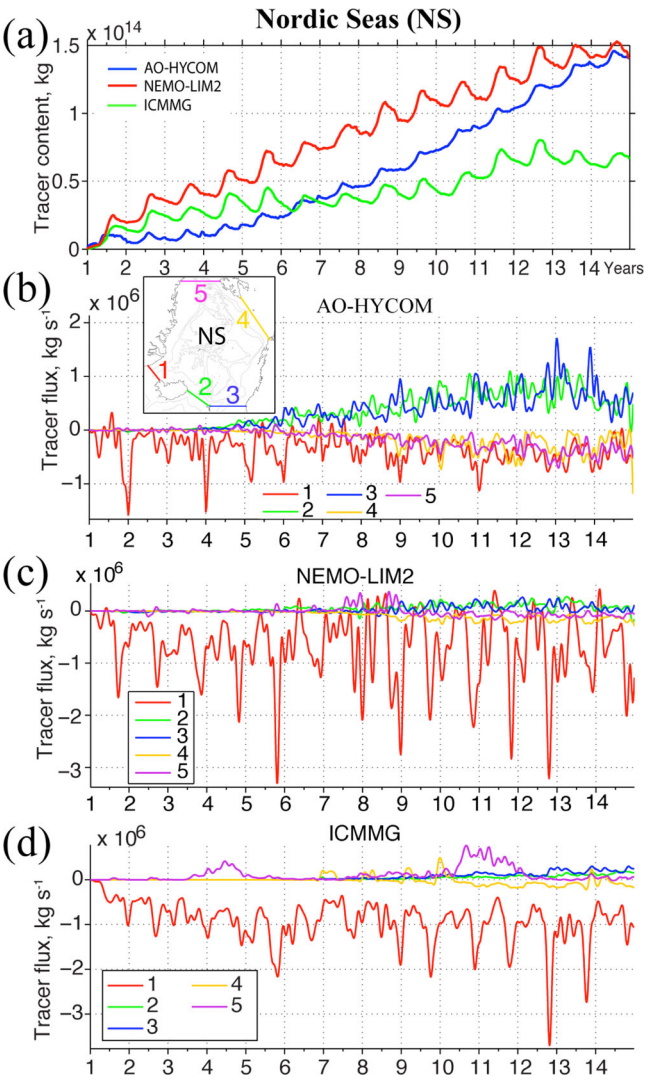

Figure 8. Tracer budget for the Nordic Seas region. (a) Volume-integrated tracer content (kg). Colors designate different models. The horizontal axis is model years. (b–d) 60 day low-pass filtered time series of the tracer fluxes (kg s^{-1}) across the sections from the model experiments. Colors designate fluxes across individual sections shown in the inset in Figure 8b. Section numbers correspond to Figure 1. Note the different scale in Figure 8b versus 8c and 8d.

4.2.1. The Nordic Seas

All models show a gradual increase of the volume-integrated tracer content signifying tracer accumulation in the Nordic Seas region over the simulation time (Figure 8a). However, the models disagree on the evolution rate of the tracer content. In the AO-HYCOM simulation, concentration of the tracer starts growing after the first 3 years. In the other two simulations, the content demonstrates a nearly steady increase over the whole integration time. All models show a negative flux across Denmark Strait (section 1) owing to the tracer export with the EGC (Figures 8b–8d); the models simulate a reasonably robust seasonal signal in this transport related to the seasonal variability in the tracer flux imposed along the Greenland coast. In AO-HYCOM (Figure 8b), the tracer net flux is negative during the first 5 years when tracers are exported out of the region. After 5 years of the simulation, tracer inflow to the Nordic Seas starts increasing through Iceland-Faroe-Shetland segments (sections 2 and 3 corresponding to the green and blue lines, respectively) and the net oceanic flux becomes positive exceeding the outflow through section 1. In NEMO-LIM2 (Figure 8c), the net flux is negative dominated by the EGC export of the

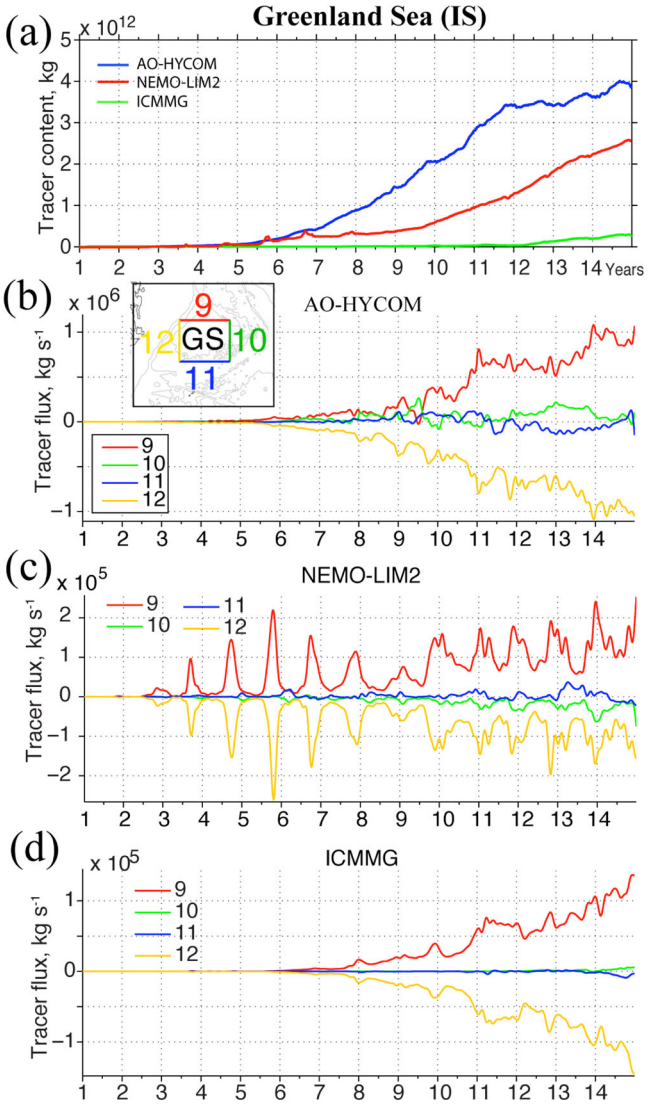

Figure 9. Same as Figure 8 but for the Greenland Sea region. Note the different scales in Figures 9b–9d.

tracer during the simulation. Contrary to the AO-HYCOM results, tracer fluxes across Iceland-Faroe-Shetland segments exhibit only minor increase after year 6. The increase in tracer content in the NS is due to the tracer advection with the East Icelandic and Jan Mayen currents in NEMO-LIM2 (Figure 6). Differing from AO-HYCOM, ICMMG (Figure 8d) simulates considerably smaller tracer inflow into NS with the North Atlantic Current through sections 2 and 3. The inflow cannot compensate tracer outflow through Denmark Strait. The imbalance in the net advective tracer fluxes is compensated by internal tracer flux along the Greenland coast, whereas in the AO-HYCOM the net advective flux is positive after 5 years indicating that tracer accumulation in the NS region is mainly attributed to the tracer advection by the North Atlantic Current.

4.2.2. The Greenland Sea

Tracer accumulation in the GS (Figure 1) deduced from the time series of the volume-integrated tracer content is largest for the AO-HYCOM model (Figure 9a). During the first 2–3 years, there is no tracer signature in the region for all models. After several years, the tracer starts spreading into the interior Greenland Sea. However, the timing and the propagation rate differ among the models. In AO-HYCOM, the tracer content starts growing after 4 years. During the last 4 years of the simulation, the accumulation rate slows down due to the fact that the tracer fluxes into and out of the box start reaching a balance. Both NEMO-LIM2 and ICMMG simulate accumulation of the tracers in the GS at a slower rate than in AO-HYCOM.

There is good agreement between the general trend of tracer fluxes in AO-HYCOM and NEMO-LIM2, with much smaller fluxes in general for the ICMMG simulations (Figures 9b and 9d). Tracer fluxes across sections 9 and 12 dominate but nearly cancel each other due to the throughflow of the recirculating Atlantic waters in the northern side of the GS. It is the balance between the fluxes through the eastern and southern sections that determines the tracer budget inside the box. In the AO-HYCOM experiment, the inflow across the eastern section (10) is mostly positive and the southern flux oscillates between positive and negative. The fluxes in ICMMG remain near zero through year 13.

Tracer fluxes across sections 9 and 12 in NEMO-LIM2 have a strong seasonal signal due to the propagation path of the tracer from the EGC (Figure 6), which has strong seasonal change in the tracer concentration related to seasonal variability of Greenland freshwater flux (Figure 2a). After year 8, the seasonal signals of the fluxes across sections 9 and 12 are superimposed on positive and negative trends, respectively, attributed to tracer that has traveled around the Subpolar Gyre and has been advected into the GS with the Norwegian Atlantic Current.

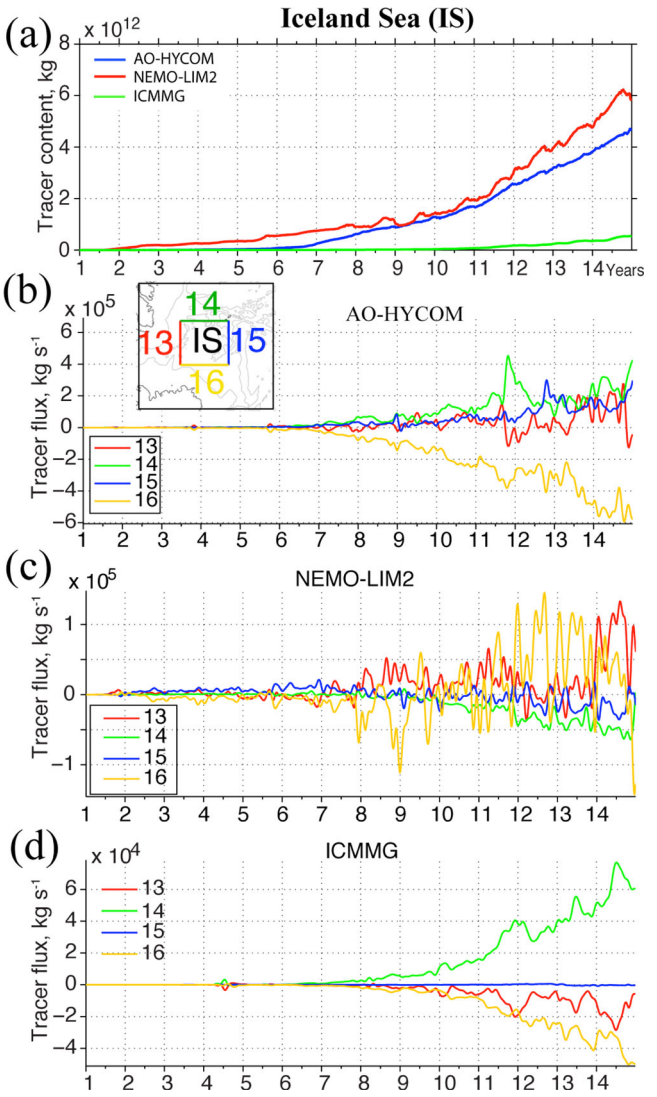

Figure 10. Same as Figure 8 but for the Iceland Sea region. Note the different scales in Figures 10b–10d.

4.2.3. The Iceland Sea

Accumulation of the passive tracer in the IS is delayed by about 1 year in NEMO-LIM2, 5 years in AO-HYCOM and 10 years in ICMMG (Figure 10a). The earlier accumulation of the tracer in the IS region in NEMO-LIM2 is related to eastward tracer transport with the East Icelandic Current (Figure 6) that is not evident in the other two simulations.

Tracer fluxes across the sections have noticeable disagreement among the models (Figures 10b–10d). AO-HYCOM simulates major tracer outflow through the southern section (16) and the inflow is mainly through the northern (14) and eastern (15) boundaries. Tracer flux through the western boundary (13) is intermittent but becomes predominantly positive by the end of the simulation. Note that after year 6, tracer flux across the southern section (16) is always negative, whereas the northern flux (14) remains positive. Similarly, ICMMG simulates persistent positive tracer flux through the northern section and negative tracer flux through the southern section (Figure 10d), however the northern inflow dominates the outflow (note the different scales). In the NEMO-LIM2 simulation, the fluxes through sections 14 and 16 are more sporadic and do not demonstrate any persistence, in contrast to AO-HYCOM and ICMMG. The oscillations across sections 13 and 16 are related to variability of the East Icelandic Current and the Jan Mayen Current that are substantial tracer sources for the interior Nordic Seas in the model.

4.2.4. The Labrador Sea

All model experiments predict an overall increase of the passive tracer content in the LS during the simulation (Figure 11a). The rate of tracer increase is similar in all simulations. Tracer fluxes across the northern (7) and southern (8) sections exhibit strong seasonality associated with seasonal changes of meltwater flux from Greenland coast (Figures 11b–11d). In AO-HYCOM and NEMO-LIM2, the southern flux through section 8 is positive during the first year of the simulation, and then it becomes predominantly negative. The shift is due to the fact that during the first year, the tracer is imported into the region with the WGC. After the tracer propagates around the Labrador Sea, it is exported out to the North Atlantic with the Labrador Current. Tracer flux between the Labrador Sea and Baffin Bay (section 7) oscillates on the seasonal time scale remaining mainly positive during the first half of the year and is reversed during the second half. Such a strong seasonal cycle is consistent with hydrographic observations in the WGC [*Myers et al.*, 2009; *Curry et al.*, 2014; *Rykova et al.*, 2015]. In the ICMMG simulation, the tracer flux across section 8 remains predominantly positive through year 10 caused by tracer influx from the North Atlantic. In contrast to the AO-HYCOM and NEMO-LIM2, the tracer is exported to Baffin Bay (through section 7) with little tracer export from the bay until year 11.

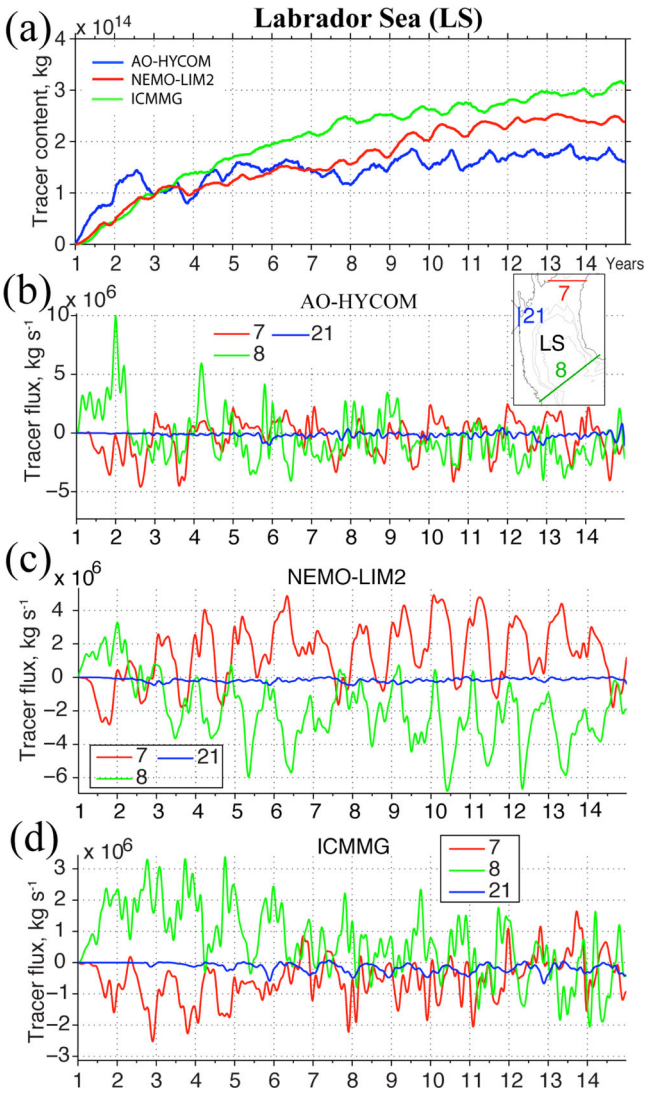

Figure 11. Same as Figure 8 but for the Labrador Sea region.

4.2.5. The Interior Labrador Sea

The rate and timing of tracer accumulation in the IL region agree between AO-HYCOM and ICMMG, whereas NEMO-LIM2 predicts a near-linear increase of the tracer until year 12 when tracer mass reaches maximum that is more than 2 times higher than in the AO-HYCOM simulation and nearly 5 times higher than in ICMMG (Figure 12a). Tracer fluxes across the sections bounding the IL box indicate different tracer advection pathways in the model experiments (Figures 12b–12d). In AO-HYCOM, the fluxes do not have any persistent pattern. On average, tracer content in the IL is determined by the influx through the eastern (section 18) and northern (17) sides and the outflows through the western (20) and southern (19) sides. The NEMO-LIM2 experiment has the strongest tracer inflow through the southern section (19), while tracer flux across the northern section (17) is primarily negative. Similar to AO-HYCOM, in ICMMG the tracer budget in the IL box is largely influenced by the flux across the eastern side (18). Tracer outflow from the IL mostly occurs through the northern section (17).

4.2.6. Baffin Bay

The BB region shows accumulation of passive tracer in all experiments with the accumulation rate differing among the models (Figure 13a). In AO-HYCOM, the tracer content rapidly increases during the first 2 years. After that, the tracer content slowly increases with superimposed seasonal variability. The NEMO-LIM2 simulation predicts faster and more persistent tracer accumulation resulting in 2 times more tracer mass by the end of the integration compared to AO-HYCOM. Results from the ICMMG experiment demonstrate a near-linear increase in the tracer content in the BB region through the simulation also exceeding twice the tracer content in the AO-HYCOM simulation by the end of the experiment. Fluxes across the northern (6) and the southern (7) sections are dominated by seasonal change (Figures 13b–13d). During the first half of the year, the tracer is advected from the Nares Strait but during the second half of the year the tracer is advected from the Labrador Sea through Davis Strait. The seasonality is attributed to wind climatology in the area with strong southerly winds in winter and weaker northerly winds in the eastern bay during summer [*Tang et al.*, 2004].

4.3. Tracer Distribution in the Labrador Sea, the Nordic Seas, and Baffin Bay

The numerical experiments illustrate that the tracer has been redistributed by ocean circulation within the entire sub-Arctic region over a relatively short time. At the beginning of the experiment, the tracer is predominantly located in the Labrador Sea and Baffin Bay (Figures 5–7). As the tracer spreads over the domain, the tracer content increases in the Nordic Seas. Analysis of the volume-integrated tracer content (section 4.2) reveals that tracer mass increases in all regions. Part of this increase is due to the overall increase of tracer mass in the domain and comparatively minor leakage of the tracer to the southern North Atlantic

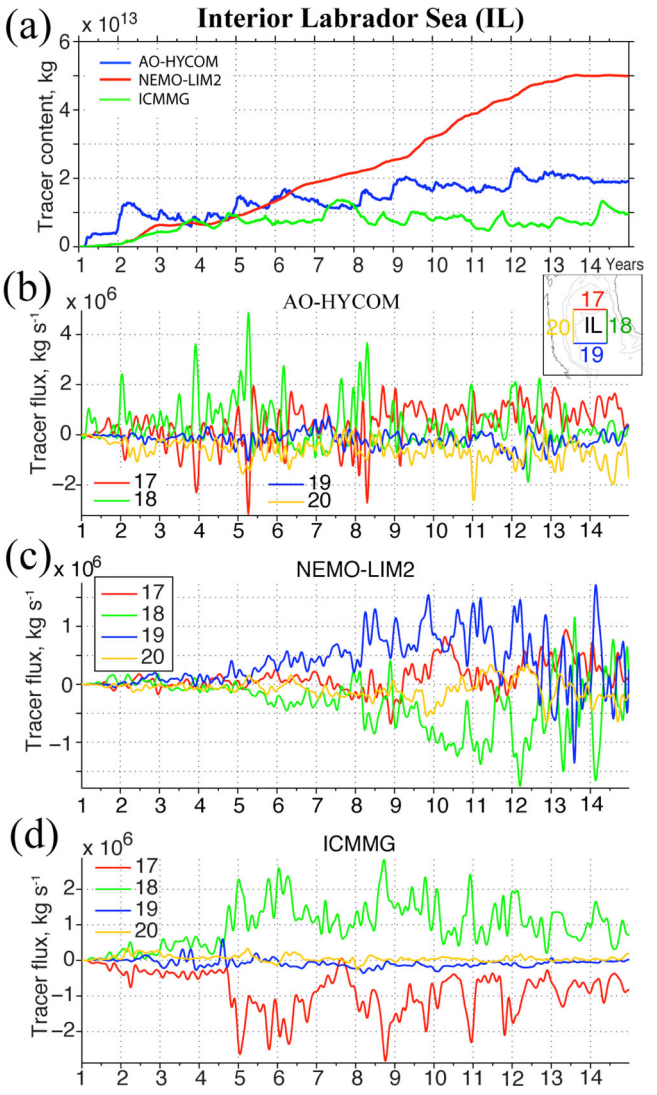

Figure 12. Same as Figure 8 but for the interior Labrador Sea region.

and the Arctic Ocean. However, the rate of tracer accumulation in the basins is also driven by the ocean circulation simulated in the models.

In order to compare the accumulation rates, the ratio of volume-integrated tracer content (mass) in the Labrador Sea, the Nordic Seas, and Baffin Bay relative to the total tracer mass released is analyzed (Figure 14). This ratio in the Labrador Sea and Baffin Bay decreases with time in all experiments. By the end of the simulations, the ratio of tracer mass in the Labrador Sea and Baffin Bay relative to the total tracer mass released is highest in the ICMMG simulation compared to the other two models. This ratio indicates that the interior Labrador Sea (Figure 14, green numbers) loses the tracer over the course of the AO-HYCOM and ICMMG simulations, while in the NEMO-LIM2 simulation there is an accumulation of tracer in the region. In the Nordic Seas, the evolution of the tracer mass ratio is in the opposite sense between the AO-HYCOM and the other two models indicating substantial differences in the simulated tracer spreading in the region. All the simulations indicate accumulation of tracer inside the GS and IS boxes (Figure 14, blue and red numbers). By the end of the simulations, the three basins contain 29.5% (AO-HYCOM), 28% (NEMO-LIM2), and 38.2% (ICMMG) of the total tracer mass. The remainder of the tracer is accumulated in the Subpolar Gyre region and in the Arctic Ocean. It is of note that the largest fraction of the tracer mass remains in the sub-Arctic seas (including the Subpolar Gyre region) after 14 years of the simulations, demonstrating that the tracer has been accumulating in the region while being transported around the sub-Arctic seas and propagating into the interior regions. The result corroborates previous studies that discuss recirculation of negative and positive salinity anomalies within the Labrador—Subpolar Gyre—Nordic Seas [*Belkin*, 2004; *Yashayaev and Seidov*, 2015].

4.4. Tracer Spreading Into the Deep Layers

Observations suggest that water masses propagate predominantly along isopycnal surfaces [e.g., *Ledwell et al.*, 1993]. Greenland freshwater spreads into the sub-Arctic seas remaining near the surface and mixing with ambient water. In the sub-Arctic seas, freshwater is mixed downward by convection and then laterally advected to distant basins [e.g., *Watson et al.*, 1999; *Rudels et al.*, 2012]. Thus, Greenland meltwater ultimately penetrates into the deep layers in the convective areas. In the numerical experiments, the tracers being released in the near-surface layer tagging buoyant meltwater quickly penetrate the subsurface layers through mechanical mixing and deep convection. Spurious diapycnal mixing can also enhance vertical propagation of the tracer in the non-isopycnal NEMO-LIM2 and ICMMG models [*Bleck*, 2002; *Hill et al.*, 2012].

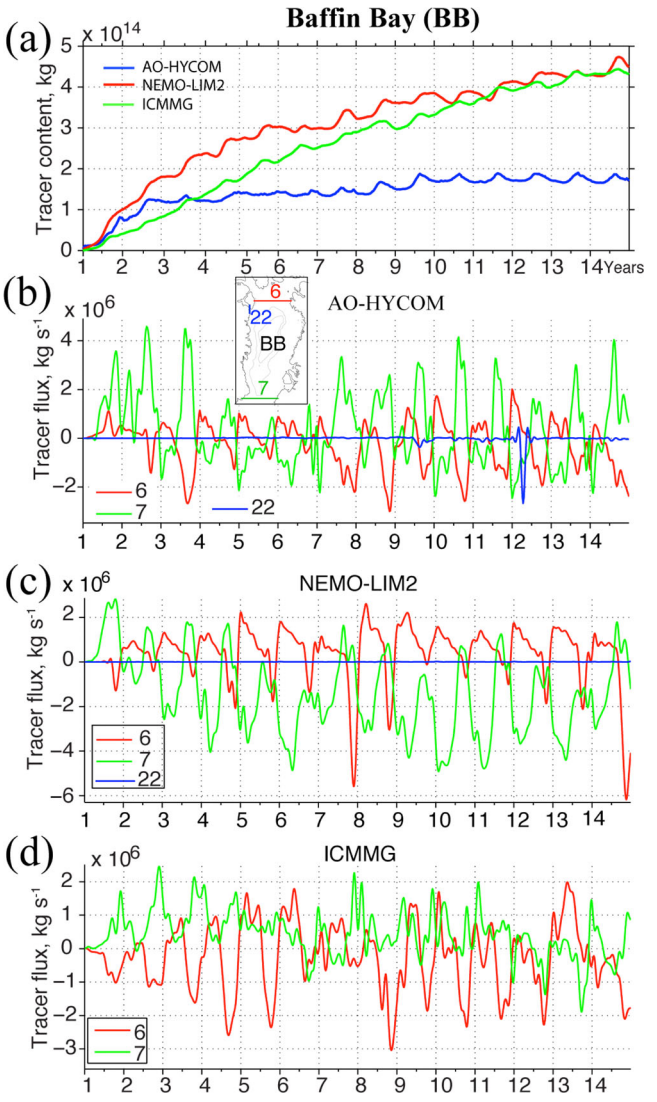

Figure 13. Same as Figure 8 but for Baffin Bay. (d) In ICMMG, section 22 is over land, thus the flux is not shown.

The models predict tracer maximum concentration in the near-surface layer (see sections in Figure 15). However, the maximum is strongly diffused in NEMO-LIM2 and ICMMG occupying depths between 200 and 500 m, by contrast, it remains within a narrow layer (upper 100 m) in AO-HYCOM. In the AO-HYCOM experiment, the deepest propagation of the tracer occurs in the North Atlantic (Figures 15a and 15b). In the Nordic Seas, the tracer is at notably shallower depths (∼800m) with distinct minima in the Greenland Sea (shallower than ∼700 m). Similarly, in Baffin Bay the tracer has not spread deeper than ∼800m. Development of deep local tracer maxima is evident in the southern Labrador Sea by the end of year 7 (also observed in Figure 14a). After 14 years of the model experiment, the passive tracer has penetrated depths exceeding 1600–1800 m in the North Atlantic including the Labrador Sea and the southern Irminger Sea. The concentration decreases with depth and is maximal in the surface layer (<200 m).

In contrast to AO-HYCOM, NEMO-LIM2 simulates tracer spreading through the whole water column in Baffin Bay (Figures 15c and 15d). In the Labrador Sea, the tracer is distributed through most of the water column down to ∼2800 m after 7 years and all the way to the bottom after 14 years. This is related to excessive Labrador Sea convection in this simulation. After 7 years, the tracer propagation shallows downstream of the North Atlantic flow with very shallow tracer signatures in the Nordic Seas owing to insufficient propagation of the tracer into this region. By the end of the simulation, the tracer spreads to the bottom in the North Atlantic and below 600 m in the Nordic Seas.

In the ICMMG experiment (Figures 15e and 15f), vertical propagation of the tracer generally agrees with AO-HYCOM. After 14 years, the model simulates deeper propagation of the tracer in the Labrador Sea and the North Atlantic basin and substantially shallower propagation in the Nordic Seas and Baffin Bay. ICMMG tracer distribution after 7 years differs from both the AO-HYCOM and NEMO-LIM2 simulations. Specifically, in ICMMG the tracer spreads deeper in the Labrador Sea, compared to the AO-HYCOM but shallower than in NEMO-LIM2. There is no tracer signature in the Nordic Seas in the ICMMG. There is good agreement in tracer depth in Baffin Bay between AO-HYCOM and ICMMG. After 14 years, tracer distribution in the North Atlantic basin in the ICMMG looks more different from AO-HYCOM. Interestingly there is no tracer in the near-surface layers in the North Atlantic basin in the ICMMG simulation, suggesting the advection origin of the subsurface tracer presence in this part of the section. The absence of the tracer in the central Labrador Sea and Nordic Seas is due to the tracer propagation with the boundary currents in this simulation.

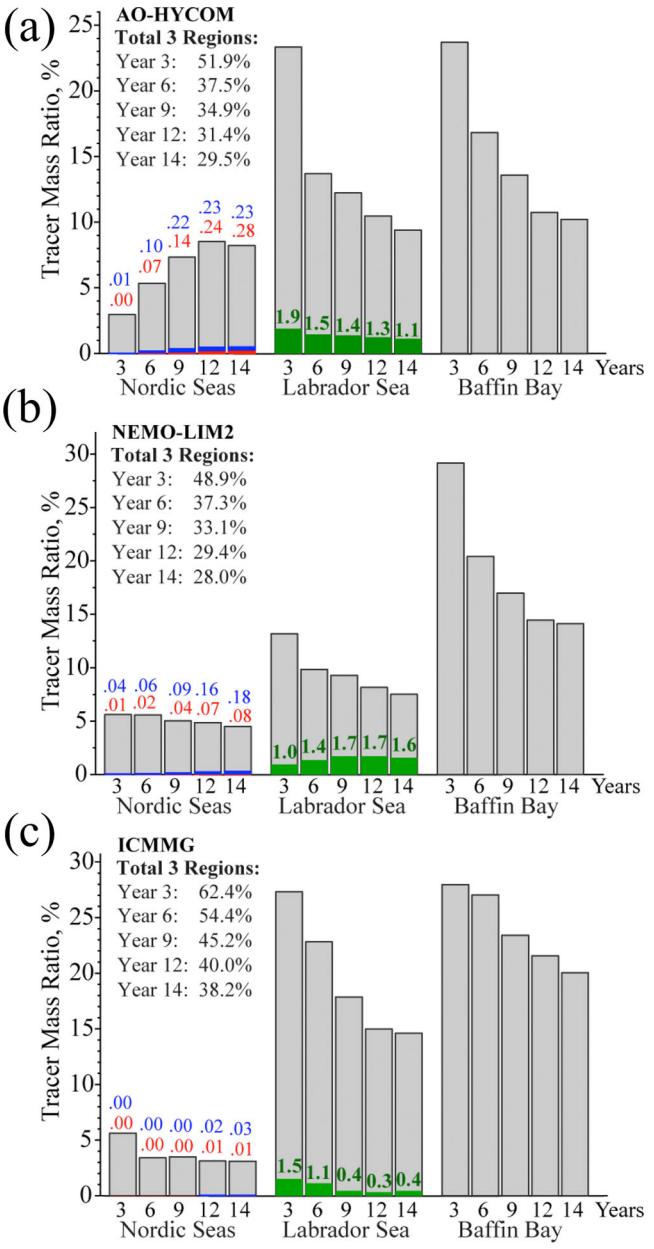

Figure 14. Mass fraction (%) of the volume-integrated tracer in three regions (NS, LS, and BB) relative to the total tracer mass integrated over the model domain (limited by ~38°N for NEMO-LIM2 and ICMMG). (a) AO-HYCOM; (b) NEMO-LIM2; (c) ICMMG. Shown are mass fraction values after 3, 6, 9, 12, and 14 years of the simulation. The colored bars inside the "Nordic Seas" and "Labrador Sea" illustrate the mass fraction of the tracer integrated over the interior boxes (blue—GS, red—IS, and green—IL) relative to the total tracer mass (the values are listed in colored numbers). Also listed is the total mass fraction of the tracer within the three regions.

5. Discussion

5.1. Pathways of Greenland Freshwater

5.1.1. Horizontal Propagation

The pathways of Greenland freshwater propagation follow the general circulation in the sub-Arctic seas (Figure 1). The tracer experiments presented demonstrate relatively rapid spreading of the passive tracer in the sub-Arctic seas within 5–7 years. Estimated travel time of the tracer in the model experiments agrees well with the estimates of propagation rates of the GSAs in the sub-Arctic inferred from observations [*Dickson et al*., 1988; *Belkin et al*., 1998; *Belkin*, 2004; *Yashayaev and Seidov*, 2015]. Based on the observed cooling and freshening signals in the region, *Dickson et al*. [1988] traced the spreading of the 1970s GSA and suggested that it took the GSA 7–8 years to propagate from Fylla Bank (off the southwestern Greenland coast) to the Norwegian Sea and 9–10 years to Spitsbergen. Upstream, propagation timescales for the GSA were 1 year longer from the eastern Greenland coast (north of Iceland). The GSAs of the 1980s and the 1990s spread faster propagating from Fylla Bank to the Norwegian Sea in about 5–6 years [*Belkin et al*., 1998; *Belkin*, 2004]. The major inflow of the tracer into the Nordic Seas in AO-HYCOM and ICMMG occurs with the North Atlantic Current. This result is in agreement with other studies where the dominant role of negative salinity anomalies carried by the Atlantic inflow on the freshening signal in the Nordic Seas has been proposed [e.g., *Glessmer et al*., 2014; *Reverdin*, 2014].

The discrepancies in the numerical solutions are apparent in tracer propagation into the interior regions of the sub-Arctic seas. There are markedly stronger horizontal gradients in tracer concentration fields simulated in ICMMG, compared to the other two models. In the coarse-resolution ICMMG simulation, the interior slowly fills with the tracer that tends to remain with the current following the boundary regions (Figure 7). For example, in ICMMG the tracer is advected into the Nordic Seas after 5 years of the simulation in agreement with the AO-HYCOM experiment, yet it takes another 7–8 years for the tracer to spread into the interior GS and IS in the ICMMG simulation compared to 2–3 years in the AO-HYCOM experiment (Figure 5). One possible reason for the observed discrepancies in the tracer distribution between ICMMG and the other two

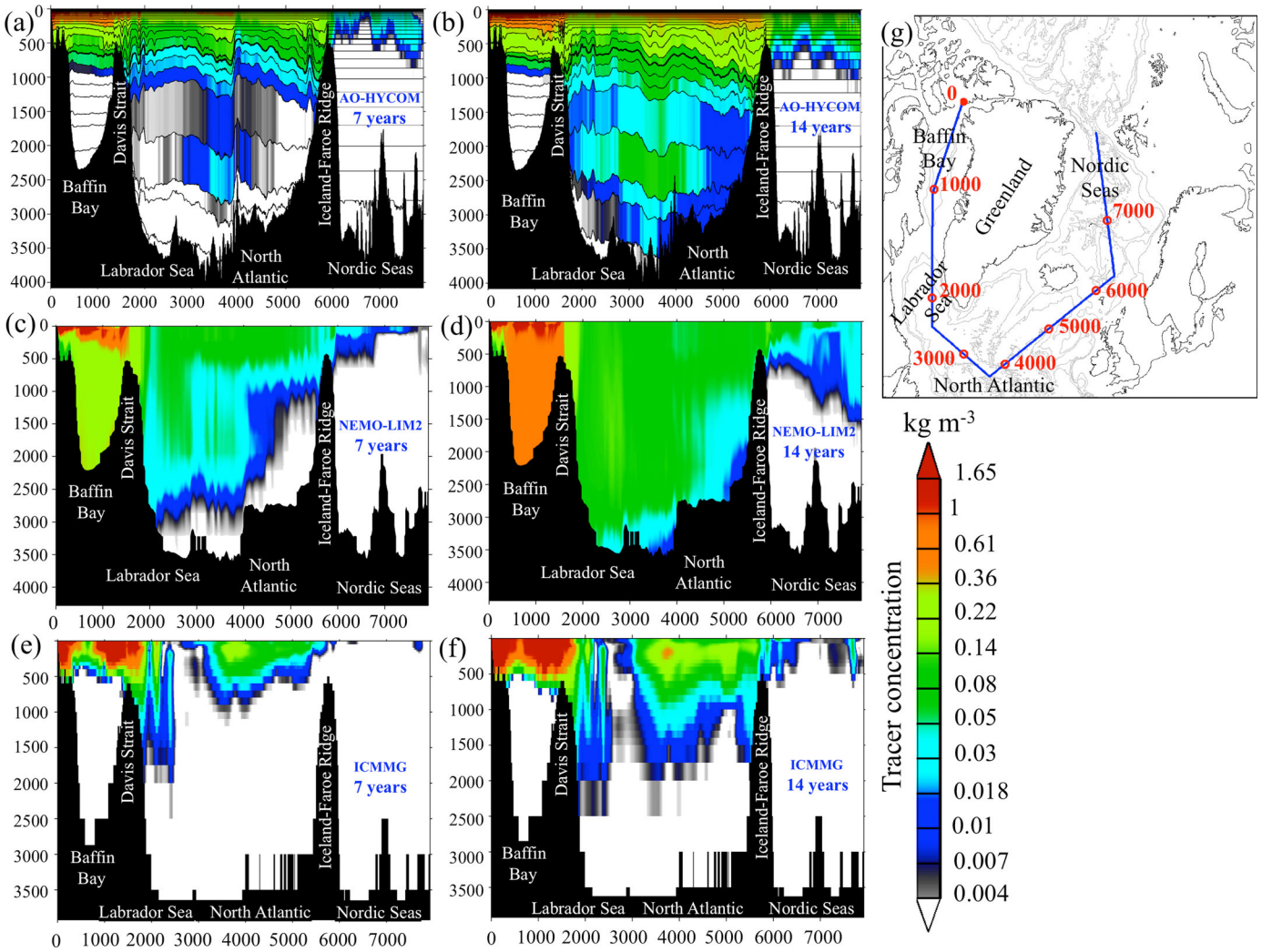

Figure 15. Distribution of the tracer concentration (kg m^{-3}) along the vertical section (g) from the numerical experiments on 17 December after 7 and 14 years. In Figures 15a–15f, the vertical axis is depth in meters. (a, b) AO-HYCOM: black contours are interfaces of the vertical layers from a single model output time. (c) NEMO-LIM2. (e, f) ICMMG. (g) Section lines. The red numbers on the blue line correspond to the distances (km) along the line also shown on the horizontal axis on the diagrams.

models could be the coarse grid spacing of the former. The coarse resolution of the ICMMG model does not permit the simulation of mesoscale eddies that may be a key mechanism for advection of tracer into the interior regions.

This assumption is supported by previous studies suggesting a leading role of small-scale eddies in lateral advection and spreading of both freshwater and Atlantic Water in the Labrador Sea [*Saenko et al.*, 2014] and the Nordic Seas [*Budeus and Ronski*, 2009; *Yashayaev and Seidov*, 2015]. For example, *Budeus and Ronski* [2009] reported a patchy distribution of Atlantic Water observed inside the Greenland Gyre. Diameters of these "Atlantic Water patches" were only 20 km with vertical extent varying from 200 to 1000 m. The findings of *Budeus and Ronski* [2009] support the idea of eddy transport of Atlantic Water into the interior Greenland Gyre (see also *Yashayaev and Seidov* [2015] for an interesting analogy of Atlantic Water circulation and a pinball machine). This view is distinct from the idea of a diffusion type of penetration that assumes gradual lateral spreading resulting in a smooth and steady transition from salinity and temperature values at the boundaries of the gyres to the interior values [e.g., *Karstensen et al.*, 2005]. This type of advection is present in the ICMMG (noneddying) simulation.

The above discussion raises the question about the meaning of "eddy-resolving" with respect to Arctic Ocean models. An "eddy-resolving" model has to be capable of adequately representing the eddy field, i.e., model horizontal grid spacing should be at least two grid points per Rossby radius of deformation and the

grid spacing is measured as the grid-diagonal distance (so called "effective spacing" in *Hallberg* [2013]). In the Nordic Seas, the first baroclinic Rossby radius of deformation is ~4–8 km [*Nurser and Bacon*, 2013]. Hence, an "eddy-resolving" model should have a grid spacing about 2–4 km. Only AO-HYCOM with 0.08° horizontal grid (effective spacing ~4–5 km in the Greenland Sea) is close to this estimate still being marginal between "eddy-resolving" and "eddy-permitting" (1 grid point per radius) [*Nurser and Bacon*, 2013]. No other model from the previous studies mentioned earlier (section 1) satisfies this resolution criterion. With >20km horizontal grid spacing, in the ICMMG model tracer propagation into the gyres is dominated by horizontal diffusion, which is much slower than transport and mixing by eddies in the other two models.

The apparent disagreement in the NEMO-LIM2 solution with the other models is that NEMO-LIM2 shows stronger tracer propagation from the EGC with the Jan Mayen Current. The causes of this intensification are not clear. We speculate that this may be related to misrepresentation of the narrow East Greenland Coastal Current, which serves as a freshwater conduit in the Nordic Seas. This problem has been discussed with respect to another 0.25° NEMO simulation in *Marsh et al*. [2010]. Alternatively, it could be due to the stronger East Icelandic Current in NEMO-LIM2 compared to the other two models.

5.1.2. Noneddying and Eddy Fluxes

The general circulation in the sub-Arctic seas follows the boundaries of the basins suggesting no tracer propagation into the interior Labrador and Nordic Seas. The AO-HYCOM and NEMO-LIM2 simulations, however, indicated tracer spreading into the interior regions (section 4) in striking contrast to the coarse-resolution ICMMG simulation that showed very minor propagation of the tracer into the interior boxes. Visual inspection of Figures 5–7 supports the rationale suggested above that different eddy activity explains the different spreading of the tracer into the interior regions. To validate this assumption, eddy tracer flux and mean (noneddying) tracer flux are calculated by separating velocities and concentration into time-mean velocity ($\bar{\mathbf{u}}$) and tracer concentration ($\bar{C}_{tr}$) and corresponding time-fluctuating components or eddy terms ($\mathbf{u}'$ and C'_{tr}). After time averaging, the tracer fluxes may be separated into mean and eddy fluxes

$$\overline{\mathbf{u}\cdot C_{tr}}=\bar{\mathbf{u}}\cdot\bar{C}_{tr}+\overline{\mathbf{u}'\cdot C'_{tr}}, \tag{3}$$

where the overbar denotes 30 day time averaging.

Figure 16 presents 1 year-averaged mean and eddy tracer fluxes for year 9 from the simulations. The mean tracer flux (Figures 16a, 16c, and 16e) highlights the pathways of the tracer in the sub-Arctic seas that follow the general large-scale circulation. The general features of the mean tracer flux are similar in the models. Yet there are notable discrepancies in the smaller-scale pathways. For example, in contrast to the higher-resolution simulations, in ICMMG boundary currents are broad occupying nearly whole Baffin Bay. At the same time, the interior Nordic Seas is nearly quiescent. Note that the mean tracer flux in the Nares Strait is northward, in contradiction to AO-HYCOM and NEMO-LIM2 (as well as the observations). The eddy tracer fluxes (Figures 16b, 16d, and 16f) are predominantly directed normal to the mean flux, indicating lateral advection of the tracer into the interior regions. All the models simulate increased eddy tracer flux along southwestern and southeastern Greenland coast. The magnitude of the eddy tracer flux in the Labrador Sea is markedly higher in AO-HYCOM compared to the other two experiments (note the natural-log scale). Also AO-HYCOM fields predict a local maximum of the eddy tracer fluxes in the Norwegian Sea that is smaller in NEMO-LIM2 and is absent in ICMMG.

Next, time-integrated eddy tracer flux (F_{eddy}) and time-mean tracer flux (F_{mean}) in the upper 150 m are calculated for the interior boxes in the Greenland, Iceland, and Labrador seas

$$F_{mean}(t)=\int_t\int_H\int_L \bar{u}_\perp\cdot\bar{C}_{tr}\,dl\,dz\,dt, \tag{4}$$

$$F_{eddy}(t)=\int_t\int_H\int_L \overline{u'_\perp\cdot C'_{tr}}\,dl\,dz\,dt, \tag{5}$$

where $u_\perp$ is the velocity component normal to the section.

Shown in Figure 17 are mean tracer flux (equation (4)) and time-integrated eddy tracer flux (equation (5)) calculated for years 8–12. All the models demonstrate modest contribution of eddy tracer flux compared to

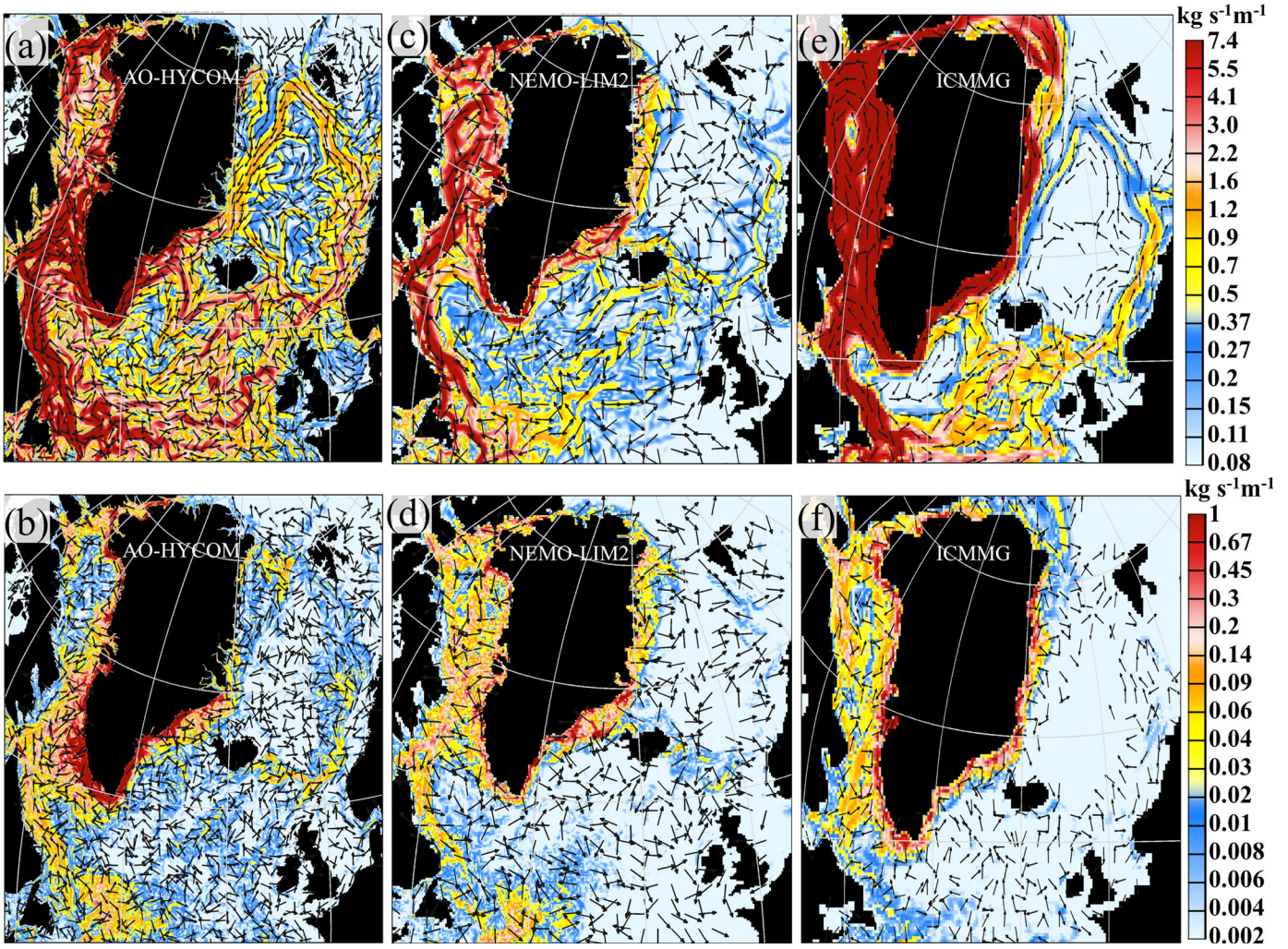

Figure 16. (top row) Mean and (bottom row) eddy tracer fluxes (kg s^{-1} m^{-1}) integrated over the upper 150 m calculated from daily-mean fields (a, b) AO-HYCOM, (c, d) NEMO-LIM2, and (e, f) ICMMG for year 9. The fluxes are 1 year averaged.

the mean flux in the Nordic Seas. This is an expected result from the previous analysis of Figure 16. Strikingly different from the Nordic Seas is the substantial contribution of eddy flux in the Labrador Sea in the AO-HYCOM simulation. The amount of tracer advected by eddies into the IL box is higher than the amount advected by the mean fluxes. This result is different from the NEMO-LIM2 and ICMMG simulations where the eddy tracer flux is negligibly small in the IL region.

Thus, analysis of the tracer fluxes simulated in the models has demonstrated the predominant role of the mean tracer flux into the interior Nordic Seas. The eddy tracer flux dominates the noneddying tracer flux in the interior Labrador Sea in the AO-HYCOM simulation. Calculated eddy fluxes do not support the idea of eddy advection as the dominant mechanism of tracer transport into the interior Nordic Seas, in contrast to the Labrador Sea.

5.2. Greenland Freshwater Influence on Salinity in the Sub-Arctic Seas From AO-HYCOM

The simulations with the passive tracer have demonstrated rapid tracer propagation over the sub-Arctic seas suggesting widespread influence of Greenland freshwater flux in the region in agreement with the hypothesis discussed in section 1. The tracer concentration increases in all the sub-Arctic seas during 14 years of model simulations indicating accumulation of Greenland freshwater in the basins. The results imply the growth of freshwater content that should manifest in increasing negative salinity anomaly in the upper sub-Arctic seas. Nevertheless, there is no obvious observational evidence that could relate freshening signals in the region with Greenland freshwater flux. According to the model results, accumulation over the

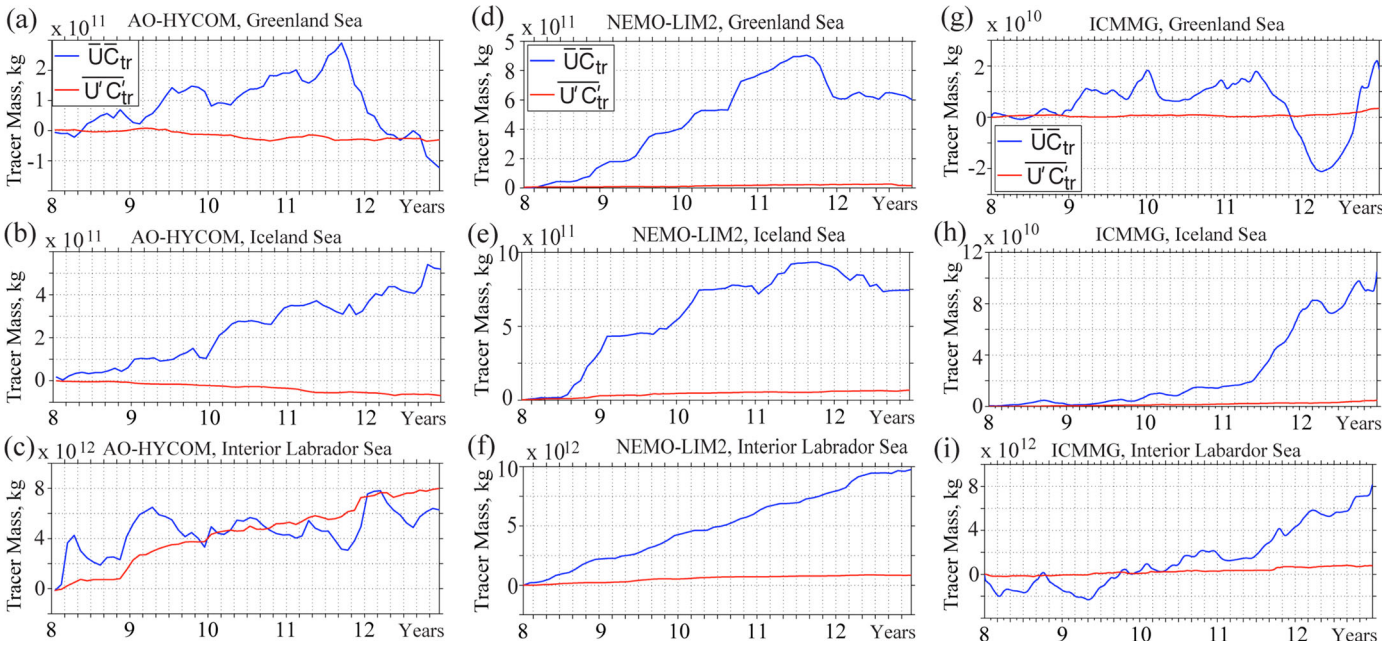

Figure 17. Mass gain (time integrated net tracer flux, kg) from the mean tracer flux (blue) and eddy tracer flux (red) into the interior convective regions (Figure 1) during years 8–12 of the simulations from (a–c) AO-HYCOM, (d–f) NEMO-LIM2, and (g–i) ICMMG. The horizontal axis is time (model years).

last two decades of surplus Greenland freshwater should have resulted in a negative salinity trend in the near-surface layer. Instead, observed salinity changes alternate between positive and negative anomalies with no persistent temporal pattern (as discussed in section 3). In the following section, the influence of the Greenland freshwater flux on salinity changes in the sub-Arctic region is analyzed using results from only the AO-HYCOM simulation, which has the highest resolution.

5.2.1. Greenland Freshwater Flux and Salinity Change in the Sub-Arctic Seas

The AO-HYCOM experiment was initialized from another simulation that had been integrated without Greenland runoff. In the tracer experiment, Greenland freshwater flux is "turned on" at the first time step of the model integration. Hence, there is a discrete jump in the freshwater forcing from the initial conditions with zero Greenland runoff to $>1000\ \mathrm{km}^{-3}\cdot\mathrm{yr}^{-1}$ (0.032 Sv) in the simulation. This provides easier detection and tracking of Greenland freshwater propagation and associated freshwater anomalies in the sub-Arctic seas. The drawback of the experiment design is that simulated negative salinity changes in the sub-Arctic seas can be too extreme for direct comparison with observational records. A better approach would be to initialize the experiment with the ocean fields from another experiment forced by realistic Greenland runoff, although in practice this still complicates the process of detection of freshwater anomalies in the basin. The AO-HYCOM results are employed here to establish relationships between Greenland freshwater flux and salinity changes in the sub-Arctic. This relationship will be used to estimate freshening in the sub-Arctic seas caused by the surplus Greenland freshwater flux in 1990–2010.

Salinity changes in the sub-Arctic basins have linear trends during the simulation (Figure 18). For every region (Figure 1), salinity is spatially averaged within the slab 0–400 m for the depths greater than 500 m. A linear relationship is sought between the spatially averaged salinity and cumulative Greenland freshwater mass Q_r

$$Q_r(t) = \int_0^t F_r \, dt, \tag{6}$$

where F_r is Greenland freshwater flux. The tracer experiments have demonstrated a delay between the time when freshwater (or passive tracer) is released at the Greenland coast and the time of appearance of the freshwater signature in the sub-Arctic basins (Figure 5). The time lag (τ) varies for the basins from 1 year for Baffin Bay to more than 5 years for the Greenland and Iceland Seas. Thus, the following regression is fit to the data

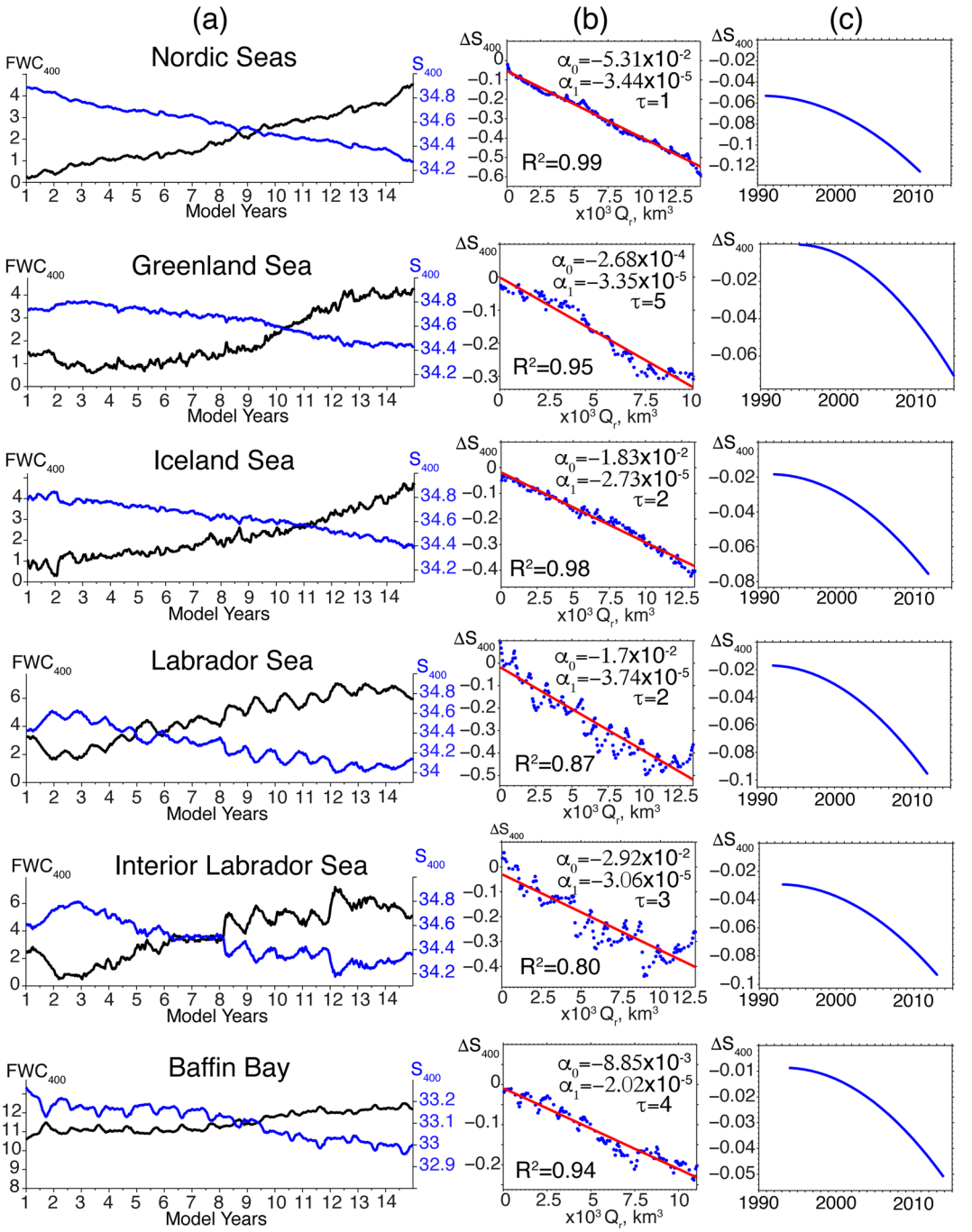

Figure 18. Hydrographic changes in the sub-Arctic regions (in rows) from AO-HYCOM. (a) Time series of freshwater content in meters (black) and salinity (blue) in the upper 400 m during the simulation. (b) Salinity change of the upper 400 m versus cumulative time-integrated Greenland freshwater flux. Linear regression parameters (equation (7)) and coefficient of determination are listed. (c) Estimated salinity change in the upper 400m for time-integrated anomaly of Greenland freshwater flux for 1990–2010.

$$dS(t) = \alpha_0 + \alpha_1 \cdot Q_r(t-\tau), \tag{7}$$

where dS is salinity change averaged in the upper 400 m within a sub-Arctic basin at time t (Figure 18b). The time lag is defined iteratively until the best fit to the data is provided, based on the highest value of the coefficient of determination (R^2). The high values of R^2 in the analyzed cases indicate a strong linear relationship between the Greenland freshwater flux and the magnitude of salinity anomaly in the regions.

The next step is to "remap" *dS* onto the observational Greenland freshwater changes reported in *Bamber et al*. [2012]. Greenland freshwater flux increased by ~200 km^3 yr^{-1} (~0.006 Sv) from 1990 to 2010. Assuming a linear increase in the Greenland freshwater flux over this period, equation (7) provides the estimated salinity change (*dS*) in the six sub-Arctic regions for 1990–2015 (Figure 18c). The magnitude of salinity anomaly is modest in the basins, especially in the interior Nordic Seas (GS and IS), suggesting a relatively small contribution of the Greenland runoff on the freshening of the sub-Arctic seas over 20 years of increased Greenland freshwater flux. According to Figure 18c, by 2010 salinity anomaly should be −0.05 in the GS, −0.07 in the IS, and −0.08 in the IL as a result of surplus Greenland freshwater flux.

An important caveat here is that salinity changes of the North Atlantic Current have not been taken into account. According to long-term observations in the Iceland-Faroe-Shetland section and in the southwestern Nordic Seas, salinity of Atlantic water increased by 0.15–0.2 in the 2000s compared to the long-term mean [*Holliday et al*., 2008; *Yashayaev and Seidov*, 2015]. Such a strong positive salinity anomaly would dominate and undermine the impact of Greenland freshwater runoff on salinity in the sub-Arctic seas. The salinity increase in the Atlantic inflow can be linked to the propagating positive salinity anomaly from the subtropical Atlantic Ocean [*Hátún et al*., 2005; *Straneo and Heimbach*, 2013].

6. Summary

As Greenland Ice Sheet melting has been accelerating, increased freshwater discharge into the ocean can have dramatic consequences for thermohaline circulation of the sub-Arctic seas. Generally accepted ramifications of the surplus freshwater flux are increased water column stability and weakening of deep convection in the interior Labrador and Nordic Seas, not to mention sea level rise as the most prominent consequence. Several hypotheses of the current and future climate changes in the Arctic and North Atlantic have been suggested on the basis of this assumption. Yet pathways and time scales of freshwater propagation in the sub-Arctic seas are not known. The influence of Greenland freshwater on convective regions remains elusive. Moreover, recent observational records demonstrate increasing salinity in the upper Nordic Seas and the Labrador Sea during the 2000s contradicting the anticipated freshening caused by accelerated Greenland Ice Sheet melt. Although freshening in the 0–200 m layer in the Labrador Sea was observed during the 2010s [*Beszczynska-Moller and Dye*, 2013; *Yashayaev et al*. 2015]. In order to address these uncertainties, three numerical experiments were conceived during FAMOS discussions. In these experiments, employing AO-HYCOM, NEMO-LIM2, and ICCMG ocean-sea ice models, a passive tracer was continuously released at Greenland freshwater source sites to track propagation of the freshwater in the sub-Arctic seas.

Results from the tracer experiments demonstrate general agreement among the models on timing and propagation of the tracer in the sub-Arctic seas. The tracer follows the large-scale ocean circulation pattern with the EGC, WGC, and the Subpolar Gyre from Greenland to the North Atlantic and with the North Atlantic Current to the Nordic Seas. The tracer quickly propagates into Baffin Bay and the Labrador Sea. The interior Labrador Sea is impacted by the tracer within the first 2 years of the simulations. The major pathway of the tracer to the Nordic Seas is via the North Atlantic Current after it has traveled around the Subpolar Gyre. It takes from 3 (AO-HYCOM) to 5 (NEMO-LIM2 and ICMMG) years for the tracer to reach the south Nordic Seas via the North Atlantic Current and another 2 years to enter convective sites in the interior Nordic Seas (except for ICMMG where tracer spreading into the interior region was not substantial over the simulation time). The Iceland Sea receives the tracer via the Iceland Current shortly after the simulation begins, yet the amount of this influx is not substantial, except in the NEMO-LIM2 simulation. Positive trends in the time series of the tracer mass inside the basins indicate that a steady state has not been reached in the simulation and the tracer was still accumulating in the sub-Arctic seas by the end of the model runs. Nevertheless, the accumulation has substantially slowed in Baffin Bay and the Labrador Sea to the end of the experiments.

The model experiments predict highest tracer concentration in Baffin Bay with the second highest concentration in the Labrador Sea. The concentration in these basins quickly reached a quasi steady state (during the first 4–5 years). In the rest of the domain, the concentration increased as the tracer propagated with the Subpolar Gyre and the North Atlantic Current towards the Nordic Seas. During the 14 year time interval, the tracer accumulated in the sub-Arctic seas. However, the simulations were not sufficiently long to reach a

steady state in tracer concentration within the domain precluding determination of the residence time of the tracer in the sub-Arctic basins.

The noticeable discrepancy in the numerical solutions is tracer propagation into the convective regions in the Labrador Sea and the Nordic Seas. In the ICMMG simulation, the interior regions are filled slowly with the tracer resulting in strong horizontal gradients of the tracer concentration, whereas the other two models simulate faster propagation of the tracer into the interior seas. The disagreement in the simulations is probably due to inability of the coarse-resolution ICCMG to represent tracer advection by small-scale eddies that may play an important role in distributing water from the currents following the margins of the sub-Arctic seas. Calculated eddy tracer fluxes demonstrated substantially higher eddy activity in the AO-HYCOM simulation, contrasting NEMO-LIM2 and ICMMG. Nevertheless, calculated eddy tracer flux into the Greenland and Iceland interior boxes did not demonstrate noticeable contribution of eddies to the total tracer flux. By contrast, eddy flux was a substantial contribution to the tracer flux into the interior Labrador Sea.

Modeled vertical distribution of tracer in the water column has a near-surface (top 200 m) maximum in the sub-Arctic seas. Simulated vertical penetration of the tracer is deepest in the North Atlantic where the tracer spreads down to the near-bottom layers in AO-HYCOM and NEMO-LIM2 and down to ~2000 m in ICMMG. The models disagree on the vertical tracer distribution in Baffin Bay where AO-HYCOM and ICMMG predict tracer penetration down to ~800 m and NEMO-LIM2 mixes the tracer all the way to the bottom. The causes of this disagreement are unclear and need further investigation.

Accumulation of the tracer in the interior regions of the sub-Arctic seas supports the idea of Greenland meltwater influence on the thermohaline processes and convection in the region. These results, however, are not directly supported by observations. No persistent negative salinity trends can be found in the reported hydrographic changes in the sub-Arctic region except for Baffin Bay. The estimates of the impact of the surplus Greenland freshwater flux on salinity changes in the upper 400 m layer suggest noticeable yet not dramatic freshening (from −0.04 to −0.12) of the sub-Arctic seas, especially in the interior regions. However, the magnitude of this freshening signal is smaller than the observed salinity increase in the Atlantic Water by 0.15–0.2 during the 2000s [*Holliday et al*., 2008]. This positive salinity anomaly counteracts the freshening signal caused by Greenland freshwater. The results of the model experiments also suggest that the accumulation of Greenland freshwater in the sub-Arctic seas caused by continuing Greenland Ice Sheet melt can amplify freshening in the Nordic Seas and the Labrador Sea during the period when salinity of the Atlantic inflow from southern North Atlantic decreases.

While the results here attest to efficient transport of freshwater derived from Greenland melt into the sub-Arctic seas, feedbacks and implications of this freshwater, as well as its relative importance with respect to influxes from the Arctic Ocean and Atlantic, remain an open question.

Appendix A: Characteristics of the Numerical Models

A1. AO-HYCOM

The high-resolution 0.08° regional Arctic Ocean HYbrid Coordinate Ocean Model (HYCOM) coupled to the Los Alamos National Laboratory Community Ice CodE (CICE) [*Hunke and Lipscomb*, 2008] is used in this application (hereinafter referenced as AO-HYCOM). HYCOM is a primitive equation generalized coordinate (hybrid) ocean model [*Bleck*, 2002; *Chassignet et al*., 2006]. The model domain is a subset of the global HYCOM [*Metzger et al*., 2014] north of ~38°N. The computational grid of the AO-HYCOM is a Mercator projection from the southern boundary to 47°N. North of 47°N, it employs an orthogonal curvilinear Arctic dipole grid [*Murray*, 1996]. The model employs 32 hybrid vertical coordinate layers with potential density referenced to 2000 m and includes the effect of thermobaricity [*Chassignet et al*., 2003]. The model is forced with atmospheric fields (2 m air temperature, 2 m atmospheric humidity, surface shortwave and longwave heat fluxes, and precipitation) that are derived from hourly fields of the Climate Forecast System Reanalysis (CFSR) [*Saha et al*., 2010]. Wind stress is estimated from the Cross-Calibrated Multi-Platform Ocean Surface Wind vector Analyses (CCMP) [*Atlas et al*., 2011]. The atmospheric fields employed for this experiment cover the period from 2004 to 2010 and have been recycled to provide forcing for 14 years. Surface latent and

Table A1. Characteristics of the Numerical Models

	AO-HYCOM	NEMO-LIM2	ICMMG
Horizontal grid	Dipole curvilinear, 0.08°	Curvilinear, 025°	Dipole curvilinear, 0.5°
Vertical coordinates	32 hybrid layers	50 geopotential levels	38 geopotential levels
Free surface	Free surface, split time step	Linear filtered free surface[a]	Rigid-lid approximation
Baroclinic time step	240 s	1080 s	5400 s
Barotropic time step	7.5 s	none	Varying
Salinity relaxation	e-Folding relaxation scale = 1.59e-8 s^{-1}.	No relaxation	No relaxation
Bathymetry	DBDBV2[b]	ETOPO1[c]+GEBCOv1[d]	2.5 km IBCAO[e]
Scalar horizontal advection	Second-order flux-corrected transport	TVD[f]	Ultimate QUICKEST[g]
Horizontal diffusion	Laplacian diffusion = $u_d \times \Delta x$, u_d for scalars = 0.005 m/s, u_d for momentum = 2.86×10^{-3} m/s. Biharmonic diffusion: $u_d \times \Delta x^3$ Momentum dissipation = 0.03 m/s	Laplacian for tracer, maximum eddy diffusivity is 300 $m^2\ s^{-1}$ (proportional to grid size); Bilaplacian for momentum, maximum eddy viscosity is −1.5e11 m^4/s (proportional to the cubic grid size)	Laplacian, 50 m^2/s
Vertical turbulence	KPP	TKE (turbulent kinetic energy) vertical mixing model	Richardson-based vertical mixing[h] and OPPS[i]
Diapycnal diffusivity	1×10^{-7}/buoyancy freq., $m^2\ s^{-1}$	None	None
Background diffusivity	$0.1 \times 10^{-4}\ m^2\ s^{-1}$	$0.1 \times 10^{-4}\ m^2\ s^{-1}$	$0.1 \times 10^{-4}\ m^2\ s^{-1}$
Background viscosity	$0.3 \times 10^{-4}\ m^2\ s^{-1}$	$1 \times 10^{-4}\ m^2\ s^{-1}$	$1 \times 10^{-4}\ m^2\ s^{-1}$
Tracer input	Relaxed to tracer concentration based on local Greenland river runoff rate		Surface mass flux
Atmospheric forcing	CCMP winds and CFSR radiative fluxes	CGRF	NCEPR
Sea ice model	CICE v.4	LIM2	CICE v.3

[a] *Roullet and Madec* [2000].
[b] Digital Bathymetric Data Base Variable Resolution (DBDBV2).
[c] Global 1 min resolution relief data set [*Amante and Eakins*, 2009].
[d] General Bathymetric Chart of the Oceans.
[e] International Bathymetric Chart of the Arctic Ocean.
[f] Total Variation Dissipation scheme [*Lévy et al.*, 2001].
[g] *Vested et al.* [1992].
[h] *Golubeva and Platov* [2007].
[i] Ocean penetrative plume scheme [*Paluszkiewicz and Romea*, 1997].

sensible heat fluxes, along with evaporation, are calculated using bulk formulas during model run time. The bulk transfer coefficients are parameterized following *Kara et al.*'s [2000] algorithm.

The model is initialized from an existing HYCOM-CICE simulation that was run with no Greenland runoff, and is integrated continuously for 14 years. Lateral open boundaries are derived from a climatology from the 0.08° Global HYCOM hindcast [*Metzger et al.*, 2014]. Thus, there is no interannual variability in the oceanic forcing superimposed at the open boundaries. It is noteworthy that surface salinity relaxation is minimal in the simulation with the e-folding relaxation scale of 1.59e-8 s^{-1} corresponding to the restoring time scale of 4 $year^{-1}$.

Greenland freshwater sources are incorporated into AO-HYCOM using monthly interannual gridded data (Figure 1b). The amount of tracer is proportional to the local freshwater flux rate and thus, tracer input replicates seasonal and interannual variability of the Greenland freshwater discharge. In HYCOM, runoff from a single source is distributed over several grid cells. From the beginning of the experiment, the passive tracer is continuously released in the upper 6 m at every model grid cell that has nonzero Greenland freshwater influx along the Greenland coast. The tracer is prescribed in the model by relaxing tracer concentration in the specified locations, which are ocean grid cells nearest to the freshwater sources along the Greenland coast, to the maximum concentration value that is defined as follows. For the given Greenland freshwater flux at some location along the coast (F_r, m^3/s), tracer concentration (kg/m^3) in the grid cell is defined as

$$C_{tr} = \frac{F_r \cdot t_{rlx} \cdot \rho_{tr}}{\Delta z \cdot \Delta x \cdot \Delta y}, \tag{A1}$$

where F_r is Greenland runoff flux at a given location ($m^3\ s^{-1}$), ρ_r is tracer density (1000 kg m^{-3}), t_{rlx} is tracer relaxation time scale (1 day, here) and Δz, Δx, and Δy are layer thickness and horizontal grid spacing (m). Tracers are released in the upper two layers in the grid cells where Greenland runoff is prescribed.

A2. NEMO-LIM2

The Nucleus for European Modelling of the Ocean model (NEMO v3.4—*Madec* [2008]) is used in this experiment. The Arctic Northern Hemisphere Atlantic configuration (ANHA4) was based on the 0.25° tripolar grid extracted from the NEMO ORCA025 configuration developed within the Mercator-Ocean and DRAKKAR collaboration [*Barnier et al*., 2006]. The model consists of 50 vertical levels with a 1 m top layer decreasing in resolution with increasing depth. The ANHA4 domain is contained within open boundaries at 20°S latitude and Bering Strait. Lateral boundaries are free slip. Lateral mixing varies horizontally according to a bi-Laplacian operator with a horizontal eddy viscosity of 1.5×10^{11} m^4 s^{-1}. For tracer lateral diffusion, the model uses an isopycnal Laplacian operator with a horizontal eddy diffusivity of 300 m^2 s^{-1}. Vertical mixing at sub-grid scales was parameterized using a turbulent kinetic energy (TKE) closure model [*Madec*, 2008; *Axell*, 2002]. Background vertical eddy viscosity and diffusivity are 10^{-4} m^2 s^{-1} and 10^{-5} m^2 s^{-1}, respectively.

The sea ice module is from the Louvain-la-Neuve sea-ice model (LIM2) [*Fichefet and Maqueda*, 1997] with a modified elastic-viscous-plastic (EVP) ice rheology [*Hunke and Dukowicz*, 1997]. No-slip and free-slip boundary conditions are applied for sea ice and ocean, respectively.

The simulations presented here were forced with interannual atmospheric data derived from the Canadian Meteorological Centre's Global Deterministic Prediction System (CGRF) [*Smith et al*., 2014] with an hourly resolution in time and a spatial resolution of 0.45° longitude and 0.3° latitude (minimal spacing is ~33 km in the Labrador Sea).

The model is initialized with the output from the GLORYS2V3 reanalysis from MERCATOR and then run from 2002 to 2010 and then recycled over 2004–2010 to provide a 14 year simulation. It is forced with monthly interannual runoff from *Dai et al*. [2009]. Greenland freshwater sources are incorporated using monthly interannual gridded data of *Bamber et al*. [2012]. Starting in January 2004, passive tracer is continuously released in the upper 10 m of the model at every freshwater source on the Greenland coast, with five tracers defined around the coasts of Greenland. The amount of tracer is proportional to the local freshwater discharge rate and thus, tracer flux replicates seasonal and interannual variability of the Greenland freshwater discharge. The local change of tracer concentration in the model grid cells is defined as

$$\Delta C_{tr} = \frac{F_r \Delta t}{\Delta z \, \Delta x \, \Delta y}. \tag{A2}$$

A3. ICMMG

A regional model of the Arctic and Atlantic Oceans of the Institute of Computational Mathematics and Mathematical Geophysics (ICCMG) is configured from 20°S in the Atlantic Ocean to 60°N in the Pacific Ocean [*Golubeva and Platov*, 2007]. The horizontal computational grid is bipolar curvilinear and has an equatorial resolution of 0.5° (minimal spacing is ~19 km in the study region). The model uses a hydrostatic primitive formulation of Navier-Stokes equations with the rigid-lid approximation. The sea ice model is version 3 of CICE [*Hunke and Lipscomb*, 2008].

The model is forced by wind stress, sensible, and latent heat fluxes, precipitation and evaporation, solar and longwave radiation derived from the NCEP/NCAR reanalysis [*Kanamitsu et al*., 2002]. Lateral open boundaries are provided by the PHC climatology (http://psc.apl.washington.edu/nonwp_projects/PHC/Climatology.html). The experiment is initialized from an existing 1948–2003 model run with no Greenland runoff. Greenland freshwater input is implemented in the model as surface mass and salt fluxes at the ocean grid cells closest to the freshwater sources on the Greenland coast. Similar to the other model experiments, the amount of tracer is proportional to the local freshwater discharge rate. Tracers are prescribed as mass flux (kg m^{-2} s^{-1}) into the near-surface layer calculated from the local runoff rate as

$$F_{tr} = \frac{F_r \rho_{tr}}{\Delta x \Delta y}. \tag{A3}$$

Acknowledgments

Davis Strait mooring observational data used in this study are available for download at http://iop.apl.washington.edu/data.html, with the time series also available through ACADIS, the repository for US Arctic Observing Network data. The study was part of U.S. National Science Foundation Freshwater Initiative (2004–2007) and the International Polar Year and Arctic Observing Network (2007–2010) programs under grants OPP0230381 and OPP0632231. Additional support was provided by the Department of Fisheries and Oceans, Canada. Hydrographic measurements (salinity, temperature, and pressure from bottle and CTD data) in the Greenland and Iceland seas from 1950 to 2010 have been used in this study are freely available from the ICES Data set on Ocean Hydrography (www.ocean.ices.dk) and the Pangaea database (www.pangaea.de). Greenland freshwater flux data analyzed in this study is that presented in *Bamber et al*. [2012] and is available on request as a gridded product. The analysis of salinity in Baffin Bay and the northern Labrador Sea has been performed on the basis of the UK Met Office Hadley Center observations data set version EN.4.1.1 [*Good et al*., 2013] (downloaded from http://www.metoffice.gov.uk/hadobs/en4/on 17 November 2015). D. Dukhovskoy was funded by NASA JPL IOVWST and ONR (N00014-15-1-2594). E. Chassignet was supported by the ONR (N00014-15-1-2594). HYCOM simulation was supported by a grant of computer time from the DoD High Performance Computing Modernization Program at NRL SSC. P.G. Myers and X. Hu were supported by NSERC grants RGPIN 227438-09, RGPIN 04357 and RGPCC 433898. G. Platov was supported by RFBR grants 13-05-00480, 14-05-00730, and 15-05-02457. A. Proshutinsky was funded by NSF grants PLR-0804010, PLR-1313614, and PLR-1203720. We thank W. Weijer (LANL) and I.M. Belkin (URI) for their thoughtful suggestions and comments.

References

Aagaard, K., and E. C. Carmack (1989), The role of sea ice and other fresh-water in the Arctic circulation, *J. Geophys. Res.*, *94*(C10), 14,485–14,498, doi:10.1029/JC094iC10p14485.

Aagaard, K., J. H. Swift, and E. C. Carmack (1985), Thermohaline circulation in the Arctic Mediterranean Seas, *J. Geophys. Res.*, *90*(C3), 4833–4846, *doi*:10.1029/JC090iC03p04833.

Agnew, T., A. Lambe, and D. Long (2008), Estimating sea ice area flux across the Canadian Arctic Archipelago using enhanced AMSR-E, *J. Geophys. Res.*, *113*, C10011, doi:10.1029/2007JC004582.

Amante, C., and B. W. Eakins (2009), ETOPO1 1 Arc-Minute Global Relief Model: Procedures, Data Sources and Analysis, NOAA Technical Memorandum NESDIS NGDC-24, Nat. Geo. Data. Cent., NOAA, doi:10.7289/V5C8276M.

Atlas, R., R. N. Hoffman, J. Ardizzone, S. M. Leidner, J. C. Jusem, D. K. Smith, and D. Gombos (2011), A cross-calibrated, multiplatform ocean surface wind velocity product for meteorological and oceanographic applications, *Bull. Am. Meteorol. Soc.*, *92*, 157–174, doi:10.1175/2010BAMS2946.1.

Avsic, T., J. Karstensen, U. Send, and J. Fischer (2006), Interannual variability of newly formed Labrador Sea Water from 1994 to 2005, *Geophys. Res. Lett.*, *33*, L21S02, doi:10.1029/2006GL026913.

Axell, L. B. (2002), Wind-driven internal waves and Langmuir circulations in a numerical ocean model of the southern Baltic sea, *J. Geophys. Res.*, *107*(C11), 3204, doi:10.1029/2001JC000922.

Bacon, S., G. Reverdin, I. G. Rigor, and H. M. Snaith (2002), A freshwater jet on the east Greenland Shelf, *J. Geophys. Res.*, *107*(C7), 3068, doi:10.1029/2001JC000935.

Bacon, S., A. Marshall, N. P. Holliday, Y. Aksenov, and S. R. Dye (2014), Seasonal variability of the East Greenland Coastal Current, *J. Geophys. Res. Oceans*, *119*, 3967–3987, doi:10.1002/2013JC009279.

Bamber, J., M. van den Boreke, J. Ettema, and J. Lenaerts (2012), Recent large increase in freshwater fluxes from Greenland into the North Atlantic, *Geophys. Res. Lett.*, *39*, L19501, doi:10.1029/2012GL052552.

Barnier, B., et al. (2006), Impact of partial steps and momentum advection schemes in a global ocean circulation model at eddy-permitting resolution, *Ocean Dyn.*, *56*(5), 543–567, doi:10.1007/s10236.

Belkin, I. (2004), Propagation of the "Great Salinity Anomaly" of the 1990s around the northern North Atlantic, *Geophys. Res. Lett.*, *31*, L08306, doi:10.1029/2003GL019334.

Belkin, I. M., S. Levitus, J. I. Antonov, and S.-A. Malmberg (1998), "Great Salinity Anomalies" in the North Atlantic, *Prog. Oceanogr.*, *41*, 1–68.

Beszczynska-Moller, A. and S.R. Dye (Eds.) (2013), *ICES Report on Ocean Climate 2012, ICES Coop. Res. Rep*. 321, 73i pp., International Council for the Exploration of the Sea, Copenhagen, Denmark.

Bleck, R. (2002), An oceanic general circulation model framed in hybrid isopycnic Cartesian coordinates, *Ocean Modell.*, *4*, 55–88.

Box, J. E., and W. Colgan (2013), Greenland ice sheet mass balance reconstruction. Part III: Marine ice loss and total mass balance (1840-2010), *J. Clim.*, *26*, 6990–7002, doi:10.1175/JCLI-D-12-00546.1.

Budeus, G. and S. Ronski (2009), An integral view of the hydrographic development in the Greenland Sea over a decade, *Open Ocean J.*, *3*, 9–40.

Carmack, E.C. (2000), Large-scale physical oceanography of polar oceans, in *The Freshwater Budget of the Arctic Ocean*, edited by E. L. Lewis et al., pp. 91–126, Kluwer Acad., Netherlands.

Castro de la Guardia, L., X. Hu, and P. G. Myers (2015), Potential positive feedback between Greenland Ice Sheet melt and Baffin Bay heat content on the west Greenland shelf, *Geophys. Res. Lett.*, *42*, 4922–4930, doi:10.1002/2015GL064626.

Chassignet, E. P., L. T. Smith, G. R. Halliwell, and R. Bleck (2003), North Atlantic simulations with the HYbrid Coordinate Ocean Model (HYCOM): Impact of the vertical coordinate choice, reference pressure, and thermobaricity, *J. Phys. Oceanogr.*, *33*, 2504–2526, doi:10.1175/1520-0485(2003)033<2504:NASWTH>2.0.CO;2.

Chassignet, E. P., et al. (2006), Generalized vertical coordinates for eddy-resolving global and coastal ocean forecasts, *Oceanography*, *19*, 20–31.

Clark, P. U., N. G. Pisias, T. F. Stocker, and A. J. Weaver (2002), The role of the thermohaline circulation in abrupt climate change, *Nature*, *415*, 863–869, doi:10.1038/415863a.

Curry, B., C. M. Lee, B. Petrie, R. E. Moritz, and R. Kwok (2014), Multiyear volume, liquid freshwater, and sea ice transports through Davis strait, 2004-10, *J. Phys. Oceanogr.*, *44*, 1244–1266.

Curry, R. G., and C. Mauritzen (2005), Dilution of the northern North Atlantic Ocean in recent decades, *Science*, *308*, 1772–1774.

Curry, R. G., R. Dickson, and I. Yashayaev (2003), A change in the freshwater balance of the Atlantic Ocean over the past four decades, *Nature*, *426*, 826–829.

Dai, A., T. Qian, K. E. Trenberth, and J. D. Milliman (2009), Changes in continental freshwater discharge from 1948 to 2004, *J. Clim.*, *22*, 2773–2791.

Dickson, R., B. Rudels, S. Dye, M. Karcher, J. Meincke, and I. Yashayaev (2007), Current estimates of freshwater flux through Arctic and subarctic seas, *Prog. Oceanogr.*, *73*, 210–230.

Dickson, R. R., J. Meincke, S.-A. Malmberg, and A. J. Lee (1988), The "Great Salinity Anomaly" in the Northern North Atlantic 1968–82, *Prog. Oceanogr.*, *20*, 103–151.

Dickson, R. R., I. Yashayaev, J. Meincke, W. Turrell, S. Dye, and J. Holfort (2002), Rapid freshening of the deep North Atlantic over the past four decades, *Nature*, *416*, 832–837.

Dukhovskoy, D. S., M. A. Johnson, and A. Proshutinsky (2004), Arctic decadal variability: An auto-oscillatory system of heat and fresh water exchange, *Geophys. Res. Lett.*, *31*, L03302, doi:10.1029/2003GL019023.

Ettema, J., M. van den Broeke, E. van Meijgaard, W. van de Berg, J. L. Bamber, J.E. Box, and R. C. Bales (2009), Higher surface mass balance of the Greenland ice sheet revealed by high-resolution climate modeling, *Geophys. Res. Lett.*, *36*, L12501, doi:10.1029/2009GL038110.

Fanning, A. F., and A. J. Weaver (1997), Temporal-geographical meltwater influences on the North Atlantic Conveyor: Implications for the Younger Dryas, *Paleoceanography*, *12*(2), 307–320, doi:10.1029/96PA03726.

Fichefet, T., and M. A. Morales Maqueda (1997), Sensitivity of a global sea ice model to the treatment of ice thermodynamics and dynamics, *J. Geophys. Res.*, *102*(C6), 12,609–12,646, doi:10.1029/97JC00480.

Fichefet, T., Poncin, C., Goosse, H., Huybrechts, P., Janssens, and I., H. LeTreut (2003), Implications of changes in freshwater flux from the Greenland Ice Sheet for the climate of the 21st century, *Geophys. Res. Lett.*, *30*(17), 1911, doi:10.1029/2003GL017826.

Gardner, A., G. Moholdt, B. Wouters, G. J. Wolken, D. O. Burgess, M. J. Sharp, J. G. Cogley, C. Braun, and C. Labine (2011), Sharply increased mass loss from glaciers and ice caps in the Canadian Arctic Archipelago, *Nature*, *473*, 357–360, doi:10.1038/nature10089.

Gerdes, R., W. Hurlin, and S. M. Griffies (2006), Sensitivity of a global ocean model to increased run-off from Greenland, *Ocean Modell.*, *12*, 416–435.
Glessmer, M. S., T. Eldevik, K. Vage, J. E. O. Nilsen, and E. Behrens (2014), Atlantic origin of observed and modeled freshwater anomalies in the Nordic Seas, *Nat. Geosci.*, *7*, 801–805.
Golubeva, E. N., and G. A. Platov (2007), On improving the simulation of Atlantic water circulation in the Arctic Ocean, *J. Geophys. Res.*, *112*, C04S05, doi:10.1029/2006JC003734.
Good, S. A., M. J. Martin, and N. A. Rayner (2013), EN4: Quality controlled ocean temperature and salinity profiles and monthly objective analyses with uncertainty estimates, *J. Geophys. Res. Oceans*, *118*, 6704–6716, doi:10.1002/2013JC009067.
Goosse, H., F. M. Selten, R. J. Haarsma, and J. D. Opsteegh (2002),A mechanism of decadal variability of the sea-ice volume in the Northern Hemisphere, *Clim. Dyn.*, *19*, 61–83, doi:10.1007/s00382-001-0209-5.
Gregory, J. M., and J. A. Lowe (2000), Predictions of global and regional sea-level rise using AOGCMs with and without flux adjustment, *Geophys. Res. Lett.*, *27*(19), 3069–3072, doi:10.1029/1999GL011228.
Hallberg, R. (2013), Using a resolution function to regulate parameterizations of oceanic mesoscale eddy effects, *Ocean Modell.*, *72*, 92–103, doi:10.1016/j.ocemod.2013.08.007.
Hátún, H., A. B. Sando, H. Drange, B. Hansen, and H. Valdimarsson (2005), Influence of the Atlantic subpolar gyre on the thermohaline circulation, *Science*, *309*, 1841–1844.
Helm, V., A. Humbert, and H. Miller (2014), Elevation and elevation change of Greenland and Antarctica derived from CryoSat-2, *Cryosphere*, *8*(4), 1539–1559.
Hill, C., D. Ferreira, J.-M. Campin, J. Marshall, R. Abernathey, and N. Barrier (2012), Controlling spurious diapycnal mixing in eddy-resoling height-coordinate ocean models: Insights from virtual deliberate tracer release experiment, *Ocean Modell.*, *45–46*, 14–26.
Holliday, N. P., et al. (2008), Reversal of the 1960s to 1990s freshening trend in the northeast North Atlantic and Nordic Seas, *Geophys. Res. Lett.*, *35*, L03614, doi:10.1029/2007GL032675.
Hu, A., G. A. Meehl, W. Han, and J. Yin (2011), Effect of the potential melting of the Greenland Ice Sheet on the Meridional Overturning Circulation and global climate in the future, *Deep-Sea Research Part II: Topical Studies in Oceanography*, *58*, 1914–1926, doi:10.1016/j.dsr2.2010.10.069.
Hunke, E. C., and J. K. Dukowicz (1997), An elastic–viscous–plastic model for sea ice dynamics, *J. Phys. Oceanogr.*, *27*, 1849–1867, doi:10.1175/1520-0485(1997)027<1849:AEVPMF>2.0.CO;2.
Hunke, E. C., and W. Lipscomb (2008), *CICE: The Los Alamos Sea Ice Model: Documentation and Software User's Manual*, Version 4.0, *Tech. Rep. LA-CC-06-012*, Los Alamos Natl. Lab., Los Alamos, N. M.
Huybrechts, P., et al. (2002), The response of the Greenland Ice Sheet to climate changes in the 21st century by interactive coupling of an AOGCM with a thermomechanical ice-sheet model, *Ann. Glaciol.*, *35*, 409–415.
Ikeda, M. (1990), Decadal oscillations of the air-ice-ocean system in the northern hemisphere, *Atmos. Ocean*, *28*, 106–139.
Ikeda, M., J. Wang, and J.-P. Zhao (2001), Hypersensitive decadal oscillations in the Arctic/subarctic climate, *Geophys. Res. Lett.*, *28*(7), 1275–1278, doi:10.1029/2000GL011773.
Jahn, A. and M. M. Holland (2013), Implications of Arctic sea ice changes for North Atlantic deep convection and the meridional overturning circulation in CCSM4-CMIP5 simulations, *Geophys. Res. Lett.*, *40*, 1206–1211, doi:10.1002/grl.50183.
Jungclaus, J. H., et al. (2006), Will Greenland melting halt the thermohaline circulation?, *Geophys. Res. Lett.*, *33*, L17708. doi:10.1029/2006GL026815.
Kanamitsu, M., W. Ebisuzaki, J. Woollen, S.-K. Yang, J. J. Hnilo, M. Fiorino, and G. L. Potter (2002), NCEP–DOE AMIP-II Reanalysis (R-2), *Bull. Am. Meteorol. Soc.*, *83*, 1631–1643, doi:10.1175/BAMS-83-11-1631.
Kara, A. B., P. A. Rochford, and H. E. Hurlburt (2000), Efficient and accurate bulk parameterizations of air-sea fluxes for use in general circulation models, *J. Atmos. Oceanic Technol.*, *17*, 1421–1438.
Karstensen, J., P. Schlosser, D. W. R. Wallace, J. L. Bullister, and J. Blindheim (2005), Water mass transformation in the Greenland Sea during the 1990s, *J. Geophys. Res.*, *110*, *C07022*, doi:10.1029/2004JC002510.
Kieke, D., and I. Yashayaev (2015), Studies of Labrador Sea Water formation and variability in the subpolar North Atlantic in the light of international partnership and collaboration, *Prog. Oceanogr.*, *132*(3), 220–232, doi:10.1016/j.pocean.2014.12.010.
Kleinen, T., T. J. Osborn, and K. R. Briffa (2009), Sensitivity of climate response to variations in freshwater hosing location, *Ocean Dyn.*, *59*, 509–521.
Kwok, R. (2007), Baffin Bay ice drift and export: 20022007, *Geophys. Res. Lett.*, *34*, L19501, doi:10.1029/2007GL031204.
Latarius, K. and D. Quadfasel (2010), Seasonal to inter-annual variability of temperature and salinity in the Greenland Sea Gyre: heat and freshwater budgets, *Tellus*, *62A*, 497–515, doi:10.1111/j.1600-0870.2010.00453.x.
Lazier, J., R. Hendry, R. Clarke, I. Yashayaev, and P. Rhines (2002), Convection and restratification in the Labrador Sea, 1990-2000, *Deep Sea Res., Part I*, *49*, 1819–1835.
Ledwell, J. R., A. J. Watson, and C. Law (1993), Evidence for slow mixing across the pycnocline from an open-ocean tracer-release experiment, *Nature*, *364*, 701–703.
Lévy, M., A. Estublier, and G. Madec (2001), Choice of an advection scheme for biogeochemical models, *Geophys. Res. Lett.*, *28*(19), 3725–3728, doi:10.1029/2001GL012947.
McCartney, M. S., and L. D. Talley (1982), The subpolar mode water of the North Atlantic Ocean, *J. Phys. Oceanogr.*, *12*(11), 1169–1188.
Madec, G. (2008), *NEMO Ocean Engine, Note du Pôle de Modélisation*, Inst. Pierre-Simon Laplace (IPSL), 209 pp., No 27, France.
Malmberg, S.-A., and S. Jonsson (1997), Timing of deep convection in the Grenland and Iceland seas, *ICES J. Mar. Sci.*, *54*, 300–309.
Manabe, S., and R. J. Stouffer (1988), Two stable equilibria of a coupled ocean-atmosphere model, *J. Clim.*, *1*, 841–866.
Manabe, S., and R. J. Stouffer (1993), Century-scale effects of increased atmospheric CO2 on the ocean-atmosphere system, *Nature*, *364*, 215–218.
Manabe, S., and R. J. Stouffer (1995), Simulation of abrupt climate change induced by freshwater input to the North Atlantic ocean, *Nature*, *378*, 165–167.
Marsh, R., D. Desbruyères, J. L. Bamber, B. A. de Cuevas, A. C. Coward, and Y. Aksenov (2010), Short-term impacts of enhanced Greenland freshwater fluxes in an eddy-permitting ocean model, *Ocean Sci.*, *6*, 749–760.
Metzger, E. J., et al. (2014), US Navy operational global ocean and Arctic ice prediction systems, *Oceanogr.*, *27*(3), 32–43.
Moore, G. W. K., K. Vage, R. S. Pickart, and I. A. Renfrew (2015), Decreasing intensity of open-ocean convection in the Greenland and Iceland seas, *Nature Clim. Change*, *5*, 877–882, doi:10.1038/NCLIMATE2688.
Münchow, A., and H. Melling (2008), Ocean current observations from Nares Strait to the west of Greenland: Interannual to tidal variability and forcing, *J. Mar. Res.*, *66*, 801–833, doi:10.1357/002224008788064612.
Murray, R. J. (1996), Explicit generation of orthogonal grids for ocean models, *J. Comput. Phys.*, *126*, 251–273, doi:10.1006/jcph.1996.0136.

Myers, P. G., and M. H. Ribergaard (2013), Warming of the polar water layer in Disko Bay and potential impact on Jakobshavn Isbræ, *J. Phys. Oceanogr.*, *43*(12), 2629–2640, doi:10.1175/JPO-D-12-051.1.
Myers, P. G., C. Donnelly, and M. H. Ribergaard (2009), Structure and variability of the west Greenland current in summer derived from 6 repeat standard sections, *Prog. Oceanogr.*, *80*(1), 93–112, doi:10.1016/j.pocean.2008.12.003
Mysak, L. A., and S. A. Venegas (1998), Decadal climate oscillations in the Arctic: A new feedback loop for atmospheric-ice-ocean interactions, *Geophys. Res. Lett.*, *25*(19), 3607–3610, doi:10.1029/98GL02782.
Nurser, A. J. G., and S. Bacon (2013), Eddy length scales and the Rossby radius in the Arctic Ocean, *Ocean Sci. Discuss.*, *10*, 1807–1831.
Paluszkiewicz, T. and R. D. Romea (1997), A one-dimensional model for the parameterization of deep convection in the ocean, *Dyn. Atmos. Oceans*, *26*, 95–130.
Peterson, I., J. Hamilton, S. Prinsenberg, and R. Pettipas (2012), Wind-forcing of volume transport through Lancaster Sound, *J. Geophys. Res.*, *117*, C11018, doi:10.1029/2012JC008140.
Pritchard, H. D., R. H. Arthern, D. G. Vaughan, and L. A. Edwards (2009), Extensive dynamic thinning on the margins of the Greenland and Antarctic ice sheets, *Nature*, *461*, 971–975, doi:10.1038/nature08471.
Proshutinsky, A., R. H. Bourke, and F. A. McLaughlin (2002), The role of the Beaufort Gyre in Arctic climate variability: Seasonal to decadal climate scales, *Geophys. Res. Lett.*, *29*(23), 2100, *doi*:10.1029/2002GL015847.
Proshutinsky, A., D. Dukhovskoy, M.-L. Timmermans, R. Krishfield, and J. Bamber (2015), Arctic circulation regimes, *Philos. Trans. R. Soc. A*, *373*, 20140160, doi:10.1098/rsta.2014.0160.
Rabe, B., H. Johnson, A. Münchow, and H. Melling (2012), Geostrophic ocean currents and freshwater fluxes across the Canadian Polar Shelf via Nares Strait, *J. Mar. Res.*, *70*, 603–640.
Rahmstorf, S. (1995), Bifurcations of the Atlantic thermohaline circulation in response to changes in the hydrological cycle, *Nature*, *378*, 145–149.
Rahmstorf, S. (2002), Ocean circulation and climate during the past 120,000 years, *Nature*, *419*, 207–214.
Rahmstorf, S. (2003), Thermohaline circulation: The current climate, *Nature*, *421*, 699 pp.
Rahmstorf, S., J. E. Box, G. Feulner, M. E. Mann, A. Robinson, S. Rutherford, and E. J. Schaernicht (2015), Exceptional twentieth-century slowdown in Atlantic Ocean overturning circulation, *Nat. Clim. Change*, *5*, 475–480, doi:10.1038/nclimate2554.
Reverdin, G. (2014), Freshened from the south, *Nat. Geosci.*, *7*, 783–784, doi:10.1038/ngeo2268.
Ridley, J. K., P. Huyberechts, J. M. Gregory, and J. A. Lowe (2005), Elimination of the Greenland Ice Sheet in a high CO2 climate, *J. Clim.*, *18*, 3409–3427, doi:10.1175/JCLI3482.1.
Rooth, C. (1982), Hydrology and ocean circulation, *Prog. Oceanogr.*, *11*, 131–149.
Roullet, G., and G. Madec (2000), Salt conservation, free surface, and varying levels: A new formulation for ocean general circulation models, *J. Geophys. Res.*, *105*(C10), 23927–23942, doi:10.1029/2000JC900089.
Rudels, B. (2011), Volume and freshwater transports through the Canadian Arctic Archipelago: Baffin Bay system, *J. Geophys. Res.*, *116*, C00D10, doi:10.1029/2011JC007019.
Rudels, B., M. Korhonen, G. Budeus, A. Beszczynska-Möller, U. Schauer, A. Nummelin, D. Quadfasel, and H. Valdimarsson (2012), The East Greenland Current and its impacts on the Nordic Seas: Observed trends in the past decade, *ICES J. Mar. Sci.*, *69*(5), 841–851, doi: 10.1093/icesjms/fss079.
Rykova, T., F. Straneo, and A. S. Bower (2015), Seasonal and interannual variability of the West Greenland Current System in the Labrador Sea in 1993–2008, *J. Geophys. Res. Oceans*, *120*, 1318–1332, doi:10.1002/2014JC010386.
Saenko, O. A., F. Dupont, D. Yang, P. G. Myers, I. Yashayaev, and G. C. Smith (2014), Role of resolved and parameterized eddies in the labrador sea balance of heat and buoyancy, *J. Phys. Oceanogr.*, *44*, 3008–3032, doi:10.1175/JPO-D-14-0041.1.
Saha, S., et al. (2010), The NCEP Climate Forecast System Reanalysis, *Bull. Am. Meteorol. Soc.*, *91*, 1015–1057, doi:10.1175/2010Bams3001.1.
Serreze, M. C., A. P. Barrett, A. G. Slater, R. A. Woodgate, K. Aagaard, R. B. Lammers, M. Steele, R. Moritz, M. Meredith, and C. M. Lee (2006), The large-scale freshwater cycle of the Arctic, *J. Geophys. Res.*, *111*, C11010, doi:10.1029/2005JC003424.
Smith, G. C., F. Roy, P. Mann, F. Dupont, B. Brasnett, J.-F. Lemieux, S. Laroche, and S. Blair (2014), A new atmospheric dataset for forcing ice–ocean models: Evaluation of reforecasts using the Canadian global deterministic prediction system, *Quart. J. R. Meteorol. Soc.*, *140*, 881–894, doi:10.1002/qj.2194.
Somavilla, R., U. Schauer, and G. Budéus (2013), Increasing amount of Arctic Ocean deep waters in the Greenland Sea, *Geophys. Res. Lett.*, *40*, 4361–4366, doi:10.1002/grl.50775.
Stammer, D. (2008), Response of the global ocean to Greenland and Antarctic ice melting, *J. Geophys. Res.*, *113*, C06022, doi:10.1029/2006JC004079.
Straneo, F. (2006), Heat and freshwater transport through the central Labrador Sea, *J. Phys. Oceanogr.*, *36*, 606–628.
Stommel, H. (1961), Thermohaline convection with two stable regimes of flow, *Tellus*, *2*, 224–230.
Stouffer, R. J., et al. (2006), Investigating the causes of the response of the thermohaline circulation to past and future climate changes, *J. Clim.*, *19*, 1365–1387.
Straneo, F., and P. Heimbach (2013), North Atlantic warming and the retreat of Greenland's outlet glaciers, *Nature*, *504*, 36–43, doi:10.1038/nature12854.
Sutherland, D., and R. S. Pickart (2008), The East Greenland Coastal Current: Structure, variability, and forcing, *Prog. Oceanogr.*, *78*, 58–77.
Swingedouw, D., P. Braconnot, and O. Marti (2006), Sensitivity of the Atlantic Meridional overturning circulation to the melting from northern glaciers in climate change experiments, *Geophys. Res. Lett.*, *33*, L07711, doi:10.1029/2006GL025765.
Sy, A., M. Rhein, J. R. N. Lazier, K. P. Koltermann, J. Meincke, A. Putzka, and M. Bersch (1997), Surprisingly rapid spreading of newly formed intermediate waters across the North Atlantic Ocean, *Nature*, *386*, 675–679.
Talley, L. D., and M. S. McCartney (1982), Distribution and circulation of Labrador Sea Water, *J. Phys. Oceanogr.*, *12*(11), 1189–1205.
Tang, C. C. L., C. K. Ross, T. Yao, B. Petrie, B. M. DeTracey, and E. Dunlap (2004), The circulation, water masses and sea-ice of Baffin Bay, *Prog. Oceanogr.*, *63*, 183–228.
Velicogna, I. (2009), Increasing rates of ice mass loss from the Greenland and Antarctic ice sheets revealed by GRACE, *Geophys. Res. Lett.*, *36*, L19503. doi:10.1029/2009GL040222.
Vested, H. J., P. Justesen, and L. Ekabjaerg (1992), Advection-dispersion modeling in three dimensions, *Appl. Math. Modell.*, *16*, 506–519.
Vizcaino, M., et al. (2008), Long-term ice sheet-climate interactions under anthropogenic greenhouse forcing simulated with a complex Earth System Model, *Clim. Dyn.*, *31*, 665–690. doi:10.1007/s00382-008-0368-7.
Watson, A. J., et al. (1999), Mixing and convection in the Greenland Sea from a tracer-release experiment, *Nature*, *401*, 902–904.
Walczowski, W., and J. Piechura (2006), New evidence of warming propagating toward the Arctic Ocean, *Geophys. Res. Lett.*, *33*, L12601, doi:10.1029/2006GL025872.

Weijer, W., M. E. Maltrud, M. W. Hecht, H. A. Dijkstra, and M. A. Kliphuis (2012), Response of the Atlantic Ocean circulation to Greenland Ice Sheet melting in a strongly-eddying ocean model, *Geophys. Res. Lett.*, *39*, L09606, doi:10.1029/2012GL051611.

Yashayaev, I. (2007), Hydrographic changes in the Labrador Sea, 1960-2005, *Prog. Oceanogr.*, *73*, 242–276.

Yashayaev, I., and J. W. Loder (2009), Enhanced production of Labrador Sea Water in 2008, *Geophys. Res. Lett.*, *36*, L01606, doi:10.1029/2008GL036162.

Yashayaev, I., and D. Seidov (2015), The role of the Atlantic Water in multidecadal ocean variability in the Nordic and Barents Seas, *Prog. Oceanogr.*, *132*, 68–127.

Yashayaev, I., D. Seidov, and E. Demirov (2015), A new collective view of oceanography of the Arctic and North Atlantic basins, *Prog. Oceanogr.*, *132*, 1–21.

Zweng, M. M., and A. Munchow (2006), Warming and freshening of Baffin Bay, 1916-2003, *J. Geophys. Res.*, *111*, C07016, doi:10.1029/2005JC003093.